

1 **Quantifying the $\delta^{15}\text{N}$ trophic offset in a cold-water scleractinian coral**
2 **(CWC): implications for the CWC diet and coral $\delta^{15}\text{N}$ as a marine N**
3 **cycle proxy**

4 Josie L. Mottram¹, Anne M. Gothmann², Maria G. Prokopenko³, Austin Cordova³, Veronica Rollinson¹,
5 Katie Dobkowski⁴, Julie Granger¹

6 ¹Department of Marine Sciences, University of Connecticut, Storrs, CT, 06340, USA

7 ²Departments of Physics and Environmental Studies, St. Olaf College, Northfield, MN, 55057, USA

8 ³Department of Geology, Pomona College, Claremont, CA, 91711, USA

9 ⁴Department of Environmental Studies, Woodbury University, Burbank, CA, 91504, USA

10 *Correspondence to:* Anne M. Gothmann (gothma1@stolaf.edu)

11 **Abstract.** The nitrogen (N) isotope composition ($\delta^{15}\text{N}$) of cold-water corals is a promising proxy for
12 reconstructing past ocean N cycling, as a strong correlation was found between the $\delta^{15}\text{N}$ of the organic
13 nitrogen preserved in coral skeletons and the $\delta^{15}\text{N}$ of particulate organic matter exported from the
14 surface ocean. However, a large offset of 8-9 ‰ between the $\delta^{15}\text{N}$ recorded by the coral and that of
15 exported particulate organic matter remains unexplained. The 8-9 ‰ offset may signal a higher trophic
16 level of coral dietary sources, an unusually large trophic isotope effect or a biosynthetic $\delta^{15}\text{N}$ offset
17 between the coral's soft tissue and skeletal organic matter, or some combinations of these factors. To
18 understand the origin of the offset and further validate the proxy, we investigated the trophic ecology of
19 the asymbiotic scleractinian cold water coral *Balanophyllia elegans*, both in a laboratory setting and in
20 its natural habitat. A long-term incubation experiment of *B. elegans* fed on an isotopically controlled
21 diet yielded a canonical trophic isotope effect of 3.0 ± 0.1 ‰ between coral soft tissue and the *Artemia*
22 prey. The trophic isotope effect was not detectably influenced by sustained food limitation. A long N
23 turnover of coral soft tissue, expressed as an e-folding time, of 291 ± 15 days in the well-fed
24 incubations indicates that coral skeleton $\delta^{15}\text{N}$ is not likely to track subannual (e.g. seasonal) variability
25 of diet $\delta^{15}\text{N}$. Specimens of *B. elegans* from the subtidal zone near San Juan Channel (WA, USA)
26 revealed a modest difference between soft tissue and skeletal $\delta^{15}\text{N}$ of 1.2 ± 0.6 ‰. The $\delta^{15}\text{N}$ of the coral
27 soft tissue was 12.0 ± 0.6 ‰, which was ~ 6 ‰ higher than that of suspended organic material that was
28 comprised dominantly of phytoplankton – suggesting that phytoplankton is not the primary component
29 of *B. elegans*' diet. An analysis of size-fractionated net tow material suggests that *B. elegans* fed
30 predominantly on a size class of zooplankton ≥ 500 μm , implicating a two-level trophic transfer
31 between phytoplankton material and coral tissue. These results point to a feeding strategy that may
32 result in an influence of regional food web structure on the cold-water coral $\delta^{15}\text{N}$. This factor should be
33 taken into consideration when applying the proxy to paleoceanographic studies of ocean N cycling.

34 1 Introduction

35 Interactions between ocean circulation and nutrient cycling modulate the marine biological carbon pump,
36 the consequent partitioning of CO₂ between atmosphere and ocean, and thus influence planetary climate on
37 centennial to millennial time scales (Sigman and Boyle 2000). The marine nitrogen (N) cycle is highly sensitive
38 to these interactions, such that knowledge of modern and ancient ocean N cycling can help illuminate drivers of
39 past climate and contextualize modern global change (*e.g.*, Altabet et al., 1994; Francois et al., 1997; Robinson
40 and Sigman 2008; Sigman et al., 1999; Kast et al. 2019).

41 The main tool to investigate the oceanic N cycle history is the nitrogen (N) isotope composition (*i.e.*, the
42 ¹⁵N/¹⁴N ratio) of particulate organic nitrogen (PON) exported from the euphotic zone and preserved in various
43 paleo-archives, including bulk sedimentary N in anoxic sediments (*reviewed by* Robinson et al. 2023). Hereafter,
44 we express the ¹⁵N/¹⁴N ratio using delta notation ($\delta^{15}\text{N}$). The $\delta^{15}\text{N}$ -PON recorded in paleo-oceanographic archives
45 reflects both regional N cycling processes and the balance of global ocean N source and sink terms (Sigman and
46 Fripiat 2019; Brandes and Devol 2002). In regions of the ocean where nitrate is quantitatively consumed, the
47 annually integrated $\delta^{15}\text{N}$ -PON exported from the surface reflects the isotopic composition of thermocline nitrate
48 (Altabet et al. 1991). The latter is influenced by the circulation history of nitrate (*e.g.*, Marconi et al., 2015), by
49 regional N₂ fixation (*e.g.*, Casciotti et al. 2008; Knapp et al. 2008) and by water column denitrification (*e.g.*,
50 Pride et al., 1999; De Pol-Holz et al., 2007). In regions with incomplete consumption of surface nitrate, such as
51 Southern Ocean, the isotopic discrimination imparted during nitrate assimilation is reflected in the $\delta^{15}\text{N}$ -PON,
52 which can be used to reconstruct the degree of surface nitrate consumption in the past (*e.g.*, Sigman et al., 1999;
53 Francois et al. 1997).

54 Accurate interpretation of the N cycle's paleo-history relies on the presumption that the $\delta^{15}\text{N}$ -PON preserved
55 in various palaeoceanographic archives is impervious to organic matter diagenesis. Bulk sedimentary $\delta^{15}\text{N}$
56 measurements are thus generally inadequate in this respect, subject to post-depositional processes (Robinson et
57 al. 2012) – barring fast-accumulating organic-rich anoxic sediments with negligible contribution from terrestrial
58 sources (*e.g.*, Altabet et al., 2002; Ganeshram and Pedersen, 1998). To circumvent this limitation, several
59 “biological” archives of the $\delta^{15}\text{N}$ -PON have been developed that are deemed resistant to diagenetic alteration.
60 These include the organic matter in diatom frustules and foraminifera tests (*e.g.*, Ren et al., 2009; Robinson
61 and Sigman, 2008) and the organic matter in proteinaceous corals (*e.g.*, Sherwood et al. 2009; Williams and
62 Grottoli 2010). Recently, the $\delta^{15}\text{N}$ of organic N enclosed within the aragonite mineral lattice of asymbiotic
63 scleractinian (stony) cold-water corals (CWCs) has been found to reflect the $\delta^{15}\text{N}$ -PON exported from the surface

64 ocean (Wang et al., 2014), offering an exciting new archive of marine N cycling (Wang et al. 2017; Li et al.,
65 2020, Studer et al., 2018; Chen et al. 2023). A robust cold-water coral archive of $\delta^{15}\text{N}$ -PON can complement the
66 existing suite of nitrogen proxies by reducing the potential biases inevitable for almost any individual proxy,
67 allowing for a broader geographic and temporal reconstruction, and increasing resolution of the proxy record.
68 Foremost, as with foraminifera and diatom shells, organic material trapped within the coral's original aragonite
69 mineral lattice is largely protected from diagenetic alteration (Drake et al. 2021), and compromised areas can be
70 avoided by inspecting the skeletons for contamination and recrystallization (e.g., borings) using microscopic
71 techniques (Gothmann et al. 2015). CWCs have a broad geographic distribution, being present in all ocean basins
72 from the surface to 5000 m (Freiwald, 2002). CWCs also offer the potential to generate high-resolution records
73 extending relatively far back in time, and corals have continuous skeletal accretion that records ocean conditions
74 at the time of growth, so the analysis of multiple individuals provides enhanced temporal resolution of long-term
75 records (Robinson et al., 2014; Hines et al. 2015). Unlike sediments containing microfossils (e.g. diatoms and
76 foraminifera) CWC skeletons are not subject to bioturbation and absolute ages of this paleoarchive can be
77 determined with decadal precision on the time scales of glacial-interglacial climate variability through U-Th
78 series dating (Cheng et al., 2000; Goodfriend et al. 1992, Robinson et al., 2014, Li et al., 2020). Remarkably,
79 individual coral samples can archive multiple seawater properties, such that a single CWC specimen can
80 potentially be used to reconstruct deep (e.g., $\Delta^{14}\text{C}$, pH, temperature, and circulation proxies such as Ba/Ca
81 and ϵNd) and surface ocean conditions ($\delta^{15}\text{N}$) at a precisely-known time (U-Th dating), making CWC unique as a
82 paleoceanographic archive (Robinson et al., 2014; Thiagarajan et al., 2014; Rae et al. 2018).

83 Yet an outstanding concern about the fidelity of the $\delta^{15}\text{N}$ of coral-bound organic N is a reported 8 - 9 ‰
84 offset between coral-bound $\delta^{15}\text{N}$ and the corresponding $\delta^{15}\text{N}$ -PON exported to regions of coral growth (Wang et
85 al. 2014). The magnitude of this offset substantially exceeds the 3 - 3.5 ‰ expected for a single trophic transfer
86 (Minagawa and Wada 1984), assuming CWC feed predominantly on algal material exported from the surface
87 ocean. Wang et al. (2014) explained the magnitude of the offset by arguing that CWCs feed on the more
88 abundant pool of surface-derived suspended organic material (SPOM), as the $\delta^{15}\text{N}$ SPOM at depth is typically
89 ~4-5‰ higher than that of sinking PON (Altabet 1988, Saino and Hattori, 1987). While CWCs are considered
90 generalists with regard to diet (e.g., Mortensen, 2001; Freiwald, 2002; Carlier et al., 2009; Maier et al. 2023), a
91 number of studies suggest that many species of CWC subsist predominantly on metazoan zooplankton prey (e.g.,
92 Naumann et al. 2011; Kiriakoulakis et al. 2005; Purser et al. 2010; Tsounis et al. 2010). A zooplankton diet
93 should result in an approximate two-level or more trophic transfer between surface PON and coral tissue (e.g.,

94 Sherwood et al. 2008), closer to the observed 8-9 ‰ offset, potentially rendering coral-bound $\delta^{15}\text{N}$ sensitive to
95 spatial and temporal differences in trophic-level food web structure. An alternative explanation for the offset is
96 that there is a large biosynthetic offset between the $\delta^{15}\text{N}$ of the CWC polyp and its skeletal tissue (Horn et al.
97 2011; Muscatine et al. 2005), assuming that CWCs' diet derives directly from sinking algal material from the
98 surface ocean. Otherwise, there could be an atypically large N isotope fractionation associated with the trophic-
99 level transfer between the coral diet and its tissue (>3-3.5‰), possibly borne out of intermittent starvation periods
100 (Doi et al., 2017), which is then passed on to the organic matrix within the coral skeleton. The gap in our
101 understanding of how corals record the $\delta^{15}\text{N}$ -PON exported from the surface ocean raises questions regarding the
102 consistency of the offset in space and time, and whether it is likely to differ among CWC species or due to intra-
103 specific variations in diet.

104 Due to the challenges of accessing deep-ocean environments, the trophic ecology of cold-water corals is
105 sparsely documented, yet is fundamental to understanding the role of CWCs in cold-water reef ecosystems and to
106 defining their utility as paleoceanographic archives of N cycling. The nature of the $\delta^{15}\text{N}$ offset between CWC
107 skeletal material and exported PON must be explained in order to further validate and potentially improve the use
108 of $\delta^{15}\text{N}$ of CWC skeletons as a proxy to reconstruct the history of exported PON and to further understand the
109 role of CWCs in benthic ecosystems. To this end, we studied *Balanophyllia elegans*, an asymbiotic scleractinian
110 cold-water coral found along the west coast of North America that grows as individual polyps (Fadlallah, 1983).
111 We investigated the following questions: a) Is there a large offset in $\delta^{15}\text{N}$ between coral polyp tissue and coral
112 skeletal tissue? b) Is there an unusually large trophic-level offset between coral tissue and coral diet? c) Does *B.*
113 *elegans* feed predominantly on suspended particulate organic matter (SPOM) *in situ*? or d) does *B. elegans* feed
114 predominantly on metazoan zooplankton, resulting in a two-level trophic transfer between coral tissue and N of
115 export? To evaluate question (a), we measured the $\delta^{15}\text{N}$ of tissue-skeleton pairs of coral samples collected in their
116 natural habitat. To evaluate question (b), we cultured *B. elegans* corals in the laboratory in experiments where
117 both the isotopic composition of food and the frequency of feeding was controlled. To evaluate questions (c) and
118 (d), we also investigated the $\delta^{15}\text{N}$ of various components of the food web at a field site where *B. elegans* are
119 found plentifully. Our observations offer novel insights on the growth and trophic ecology of *B. elegans*,
120 providing unique new data on the N metabolism of CWC and their feeding ecology. We contextualize our
121 conclusions to inform the use of CWC archives as a paleo-proxy for marine N cycling and ocean
122 biogeochemistry.

123

124 2. Methods

125 2.1 Collection of live coral specimens

126 Individual specimens of the cold-water coral *Balanophyllia elegans* were collected during four sampling
127 campaigns in March and June 2019, and September and November 2020 from the San Juan Channel near the
128 University of Washington's Friday Harbor Laboratory off the coast of Washington State in the Salish Sea (48.5°
129 N, -123.0° W; Figure 1). *B. elegans* is a solitary, asymbiotic cold-water cup coral native to the Pacific Northwest
130 that can be found both in shallow rocky environments and at depths as great as 500 m (Durham and Barnard
131 1952). The genus *Balanophyllia* is cosmopolitan and fossil samples as old as Eocene in age have been used for
132 paleoenvironmental study (Muhs et al. 1994; Gothmann et al., 2015; Gagnon et al. 2021). *B. elegans*'s presence
133 at near surface depths makes it an easy target for culture experiments, and *Balanophyllia sp.* can be found co-
134 occurring with the similar but more widely applied cold-water coral archive, *Desmophyllum dianthus* (Margolin
135 et al. 2014). Therefore, we consider the asymbiotic *Balanophyllia sp.* to be generally representative of other deep
136 cold-water coral species.

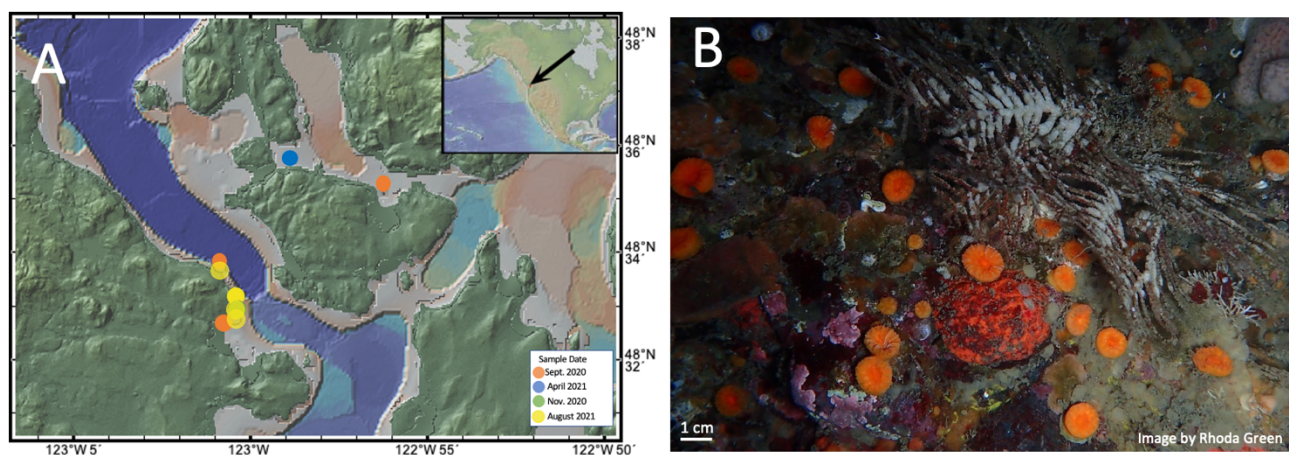


Figure 1. (a) Map of the San Juan Islands indicating the collection site of *B. elegans* specimens and hydrographic measurements (created using <http://www.geomapapp.org>, Ryan et al. 2009). Inset shows where the San Juan Islands are situated within North America. (b) Image of *B. elegans* from the San Juan Channel near Friday Harbor Labs taken by Rhoda Green.

137 *B. elegans* specimens were collected at 10 to 20 m depth by divers who gently removed the corals from
138 vertical rock walls using blunt-tipped diving knives. Of the live corals collected, a subset was immediately frozen
139 at -18°C for N isotope ratio analyses of soft tissue and organic matter bound in the coral skeleton matrix. Live
140 specimens were shipped overnight in small bags of seawater on ice to St. Olaf College (Minnesota, USA). Corals

141 were cleaned by gently scraping the exposed skeleton with dental tools to remove encrusting organisms and
142 placed in incubation bottles with artificial seawater for recovery prior to feeding experiments (described below).

143 2.2 Live coral maintenance

144 Live *B. elegans* corals were maintained in artificial seawater medium prepared from nitrate-free Instant
145 Ocean® Sea Salt. Salts were dissolved in deionized water to a salinity of 28.0 ± 0.25 – akin to the conditions at
146 the collection site (Murray et al., 2015) – and sparged with air to achieve atmospheric equilibrium. The pH of the
147 seawater was measured with a YSI brand 4130 pH probe and adjusted using dilute (0.1 N) hydrochloric acid or
148 sodium hydroxide to 8.14 ± 0.05 , slightly higher than *in-situ* conditions to promote skeletal growth. Batch
149 seawater was then allotted to 2 L airtight polypropylene bottles to incubate single coral polyps. Bottles were pre-
150 cleaned with fragrance-free soap and multiple rinses of deionized water. The salinity, pH, and temperature in the
151 incubation bottles were monitored using YSI brand probes (4310(W) conductivity cell and pH probe,
152 respectively) as well as dissolved oxygen concentrations using an optical sensor (FDO 4410; Figure S1); a
153 Multilab 4010-3w was used as the digital meter for the sensors. The bottles containing individual corals were
154 randomly distributed among three recirculating water baths maintained at a constant temperature of 12.5 ± 0.2 °C,
155 akin to the conditions at the collection site (Murray et al., 2015). Small but quasi-systematic differences of \pm
156 0.3 °C were observed among the three recirculating tanks (Figure S2). Corals were sustained on a diet of *Artemia*
157 *salina* nauplii (described below), fed twice a week to ensure maximum growth (Crook et al., 2013). Seawater in
158 the incubation bottles was replaced twice a week after the corals were fed, based on observations indicating that
159 seawater pH in the bottles decreased slightly but significantly by ~ 0.03 pH units over three days due to coral
160 respiration (statistical analysis was performed with RStudio; Welch two sample t-test; $t(515.07) = 12.8$; p-value $<$
161 0.01 ; Figure S3). Dissolved oxygen concentrations remained near atmospheric equilibrium at concentration of 7.5
162 ± 0.3 mg L⁻¹ (Figure S1). Nitrate concentrations in the bottles were also monitored from samples taken during
163 each water change, in the freshly prepared seawater and in spent seawater, revealing low variability in NO₃⁻
164 concentration of 0.7 ± 0.3 μmol L⁻¹ (Figure S4). Nitrate concentrations in the incubations were notably lower than
165 ambient levels at the collection site, where concentration were ~ 25 μmol L⁻¹, ensuring that the coral's only source
166 of nitrogen was the *Artemia* diet (Murray et al., 2015).

167 2.3 Coral culture experiments

168 2.3.1 *Experiment to quantify the trophic isotope effect*

169 The corals were acclimated to precise incubation conditions for approximately 20 hours before initiating
170 feeding experiments. To assess the $\delta^{15}\text{N}$ of coral soft tissue compared to that of its food source, four experimental
171 groups of individual *B. elegans* corals were fed respective diets of *Artemia salina* nauplii with different $\delta^{15}\text{N}$
172 values, twice per week for 530 days (Spero et al., 1993). Unhatched *Artemia salina* sourced from specific
173 geographic locations have widely different $\delta^{15}\text{N}$ values, owing to the different N isotope dynamics of the
174 environments from which they were collected, which makes these organisms useful for trophic studies (Spero et
175 al. 1993). Eighteen coral specimens were fed *Artemia* nauplii hatched from cysts from the Great Salt Lake
176 (Reference Code: GSL) with a $\delta^{15}\text{N}$ of 17.0 ± 0.3 ‰. Twelve corals were fed hatched nauplii from Lake Ulzhay
177 in Russia (Reference Code: 1816) with a $\delta^{15}\text{N}$ of 13.8 ± 0.4 ‰. Twelve corals were fed hatched nauplii from
178 Vinh Chau in Vietnam (Reference Code: 1805) with a $\delta^{15}\text{N}$ of 9.9 ± 0.3 ‰. Twelve corals were fed hatched
179 nauplii from Tibet (Reference Code: 1808) with $\delta^{15}\text{N}$ of 6.3 ± 0.2 ‰. The GSL *Artemia* was procured from
180 Aquatic Foods California Blackworm Co. (Great Salt Lake), whereas all other *Artemia* were obtained from the
181 Artemia Reference Center (Ghent, Belgium). The $\delta^{15}\text{N}$ of the diet for each treatment was calculated as the mean
182 value measured from each group of unhatched cysts and hatched nauplii (Table S2 and S3).

183 Fresh batches of nauplii were hatched from *Artemia* cysts at approximately monthly intervals, filtered into a
184 concentrated suspension, stored frozen at -18°C , and thawed immediately before feeding to the corals. Due to low
185 hatch rates of the *Artemia* group 1808, corals in that treatment group were fed nauplii harvested from
186 decapsulated *Artemia* cysts from day 151 (November 19, 2019) to 245 (February 22, 2020). The $\delta^{15}\text{N}$ of the
187 hatched nauplii ranged from 6.3 ± 0.2 to 17.0 ± 0.3 ‰ (measured by EA-IRMS; Table S2). The $\delta^{15}\text{N}$ of the
188 nauplii did not change significantly over prolonged storage of several months in the freezer (ANOVA test; $F(1) =$
189 0.07 , p -value = 0.80 ; Figure S5). *Artemia* nauplii had a statistically indistinguishable molar C:N ratios among
190 regional groups, averaging 6.0 ± 0.6 (ANOVA test; $F(3) = 0.31$; p -value = 0.82 , Table S3). These results show
191 that there was limited variability in the diet of corals due to freezer storage and hatching of multiple individual
192 batches of *Artemia* (Table S2, S3, Figure S5).

193 Corals were fed their respective nauplii diets by transferring coral individuals from their incubation bottle to
194 a small dish filled with artificial seawater with minimal exposure to air so as not to stress the corals. Each coral
195 was fed $20 \mu\text{L}$ of thawed nauplii suspension by pipetting the food directly into their oral cavity, making it
196 possible to visually ensure complete consumption and thus minimize variability in feeding rates. Each coral was

197 returned to its bottle with a fresh allotment of seawater when its mouth had remained closed for several minutes,
198 signifying that it was finished eating (Figure 2).

199 After a shift in the $\delta^{15}\text{N}$ of diet, it is expected that coral tissue $\delta^{15}\text{N}$ will evolve as a function of time until the
200 composition of tissue reaches an equilibrium in line with the new diet. In order to assess the rate (referred to here
201 as the isotopic turnover time) at which this evolution occurs, individual corals were sacrificed at discrete intervals
202 throughout the experiment. Corals were always sacrificed three days after feeding to ensure that no food
203 remained in the oral cavity. The corals were removed from their bottles and rinsed with artificial seawater. The
204 coral tissue was then separated from the skeleton using a fine stream of compressed air. The tissue and skeleton
205 were frozen at -18°C and stored separately until processed for isotope ratio analyses.

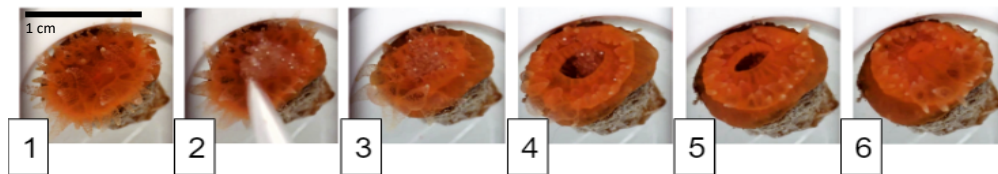


Figure 2. Photo illustration of a coral feeding sequence. Photo 1 shows coral before food is given. Photo 2 shows food being pipetted onto coral mouth. Photos 3 through 6 show the coral feeding as the mouth opens to engulf food and closes when finished, about 15 minutes in total. Corals are ~ 1 cm in diameter.

206 2.3.2 Experiment to evaluate the effects of starvation conditions

207 An additional 522-day feeding experiment was performed to assess the influence of starvation on the $\delta^{15}\text{N}$ of
208 the coral soft tissue. Live corals collected during a sampling campaign at the end of November 2020 and shipped
209 live to St. Olaf College were randomly assigned to two treatment groups (starved and not-starved). Corals in the
210 starved treatment were fed at 25% of our normal feeding frequency, or every two weeks, whereas those in the
211 not-starved treatment were fed twice a week. These feeding regimes were chosen based on the work of Crook et
212 al. (2013) and Beauchamp et al. (1989), who assumed feeding every 3 days to represent plentiful food supply and
213 feeding every 21 days (close to our starvation condition) to represent minimal maintenance food supply. Both
214 groups were fed *Artemia nauplii* with a $\delta^{15}\text{N}$ of 9.9 ± 0.3 ‰, approximately 3 ‰ lower than the coral tissue of
215 average *B. elegans* collected from Friday Harbor, and thus presumably closest in $\delta^{15}\text{N}$ to what the corals is eating
216 in the wild given a canonical trophic isotope effect. Coral incubations and feedings were conducted as described
217 above. Individuals were sacrificed over the course of the 522-day experiment, and tissue samples were frozen at -
218 18°C until isotope analysis.

219 2.4 Coral preparation for isotope ratio analyses

220 Frozen coral tissue samples (and hatched nauplii) were freeze-dried using a Labconco FreeZone 4.5 and then
221 powdered using a mortar and pestle. The samples were sent to the University of Connecticut, Avery Point
222 (Groton, CT, USA) for isotope ratio analyses.

223 Coral skeletons from specimens collected at Friday Harbor were separated from the coral soft tissue and were
224 rinsed and individually and ultrasonicated two times in Milli-Q™ (MQ) water for 20 minutes each in order to
225 remove any residual seawater. Samples were then individually ultrasonicated in a 1% sodium hypochlorite
226 (bleach) solution for at least two 20-minute intervals with fresh bleach for each new ultrasonication interval until
227 no tissue remained on the skeleton, as assessed visually under a dissection microscope. Individual skeletons were
228 then rinsed and ultrasonicated for 20 minutes in MQ another three times (each time with a new batch of MQ
229 water) in order to remove any bleach residue. Skeleton samples were sent to Pomona College (California, USA)
230 for further processing.

231 It is necessary to isolate organic matter from the coral carbonate matrix in advance of the N isotope
232 measurement methods used here (see Section 2.6 below). Organic material in the skeleton matrix was isolated
233 and oxidized to nitrate following the protocol of Wang et al. (2014). Briefly, bulk samples weighing 50-100 mg
234 were ground into coarse powder, and a fraction between 63 and 200 μm was collected by sieving through two
235 metal sieves. The 10-15 mg of sieved powder was rinsed sequentially with of sodium polyphosphate-sodium
236 bicarbonate buffered dithionite-citrate reagent, then treated with 13.5% sodium hypochlorite overnight on a
237 shaker. Skeletal material was dissolved in 4 N ultrapure hydrochloric acid, then oxidized to nitrate by autoclaving
238 in basic potassium persulfate solution. Standards of glutamine reference material USGS-40 and USGS-41
239 (respective $\delta^{15}\text{N}$ of 4.52 ‰ vs. air and 47.57 ‰ vs. air) were oxidized in tandem and used to correct for
240 processing blanks. The resulting nitrate samples were sent to the University of Connecticut for nitrate isotope
241 ratio analysis. The long-term averaged reagent blank was 0.4-0.6 $\mu\text{mol L}^{-1}$, while the typical samples were 10-15
242 $\mu\text{mol L}^{-1}$ (typical amount of nitrogen in skeleton being 2-5 $\mu\text{mole/g}$ of aragonite). Samples were typically run in
243 duplicates with an average reproducibility of $\sim \pm 0.5$ ‰. An internal laboratory standard of ground material of the
244 cold-water colonial scleractinian coral *Lophelia pertusa* had a long-term $\delta^{15}\text{N}$ value 9.4 ± 0.8 ‰ (n=57)

245 2.5 Hydrographic data

246 To infer the natural food source of the *B. elegans*, we collected samples for analysis of the $\delta^{15}\text{N}$ of particulate
247 and dissolved N pools in relation to ambient hydrographic variables (temperature and salinity) near Friday

248 Harbor, WA. Seasonal sampling campaigns were conducted in September and November 2020 and in April,
249 June, and August 2021 (Table S1). In all but the August 2021 campaign, particulate and dissolved N samples
250 were collected by divers at unspecified depths between the surface and the depth of coral collection. Samples
251 were stored frozen in 30 mL HDPE bottles. Surface net tows were performed with a mesh size of 120 μm ;
252 materials were stored and shipped frozen and thawed at a later time to be filtered onto pre-combusted GF/F filters
253 (0.7 μm nominal pore size) that were stored frozen pending isotope analysis. No hydrographic variables were
254 recorded during the campaigns except in August 2021.

255 During the August 2021 campaign, depth profiles of temperature and salinity from the surface to 35 m were
256 characterized with a CastAway®-CTD (conductivity temperature depth) profiler. Water samples were collected
257 at 5 m intervals between 5 and 30 m using a Van Dorn water sampler. Water was filtered onto pre-combusted
258 glass fiber filters (GF/F; 0.7 μm nominal pore size) into pre-cleaned 30 mL HDPE bottles and stored frozen
259 pending analyses of nitrate concentrations and nitrate isotope ratios. The corresponding filters were stored frozen
260 for isotope ratio analysis of suspended particulate organic material (SPOM). Surface (5 m) and deeper (25 m to
261 the surface) net tows were conducted using plankton nets with respective mesh sizes of 150 μm and 80 μm . Net
262 tow material was filtered directly onto a pre-combusted GF/F filters and frozen pending analysis. A portion of the
263 net tow material from the August 2021 campaign was sieved to separate size classes of 80-100 μm , 100-250 μm ,
264 $\geq 250\mu\text{m}$, 250-500 μm , and $\geq 500 \mu\text{m}$. Material from the respective size classes was filtered onto pre-combusted
265 GF/F filters and frozen until isotope analysis.

266 2.6 Nitrate concentrations and isotope ratio analyses

267 Nitrate concentrations of oxidized coral skeletons and in aqueous samples were measured by reduction to
268 nitric oxide in hot vanadium III solution followed by chemiluminescence detection of nitric oxide (Braman and
269 Hendrix, 1989) on a Teledyne chemiluminescence NO_x analyzer Model T200 (Thousand Oaks, CA).

270 The $\delta^{15}\text{N}$ and $\delta^{13}\text{C}$ of lyophilized coral tissue samples were analyzed at the University of Connecticut on a
271 Costech Elemental Analyzer–Isotope Ratio Mass Spectrometer (Delta V) and are expressed in standard delta
272 notation (e.g. for N, $\delta^{15}\text{N}$ (‰ vs. air) = $[(^{15}\text{N}/^{14}\text{N}_{\text{sample}})/(^{15}\text{N}/^{14}\text{N}_{\text{air}})] - 1$]*1000). Approximately 0.75 mg of
273 lyophilized sample (35 μg N) was allotted into tin cups and analyzed in tandem with recognized glutamine
274 reference materials USGS-40 and USGS-41 with respective $\delta^{15}\text{N}$ (vs. air) of 4.52 ‰ and 47.57 ‰ and $\delta^{13}\text{C}$ of -
275 26.39 ‰ and 37.63 ‰ (vs. PDB). Replicate analyses of ($n \geq 2$) reference materials yielded an analytical precision
276 of (± 1 SD) of 0.3 ‰ for both $\delta^{15}\text{N}$ and $\delta^{13}\text{C}$.

277 Nitrate N (and O) isotope ratios of aqueous seawater samples and N isotope ratios of the skeleton matrix
278 samples were analyzed at University of Connecticut using the denitrifier method (Casciotti et al., 2002; McIlvin
279 and Casciotti, 2011; Sigman et al., 2001). Nitrate sample solutions were injected at target concentrations of 20
280 nmol for seawater samples and 7 nmol for skeleton matrix samples. N₂O was extracted, concentrated and purified
281 using a custom-modified Thermo Gas Bench II equipped with a GC Pal autosampler and dual cold traps and
282 analyzed on a Thermo Delta V Advantage continuous flow isotope ratio mass spectrometer (Casciotti et al., 2002;
283 McIlvin and Casciotti, 2011). Individual analyses were referenced to injections of N₂O from a pure gas cylinder
284 and standardized through comparison potassium nitrate reference materials International Atomic Energy Agency
285 nitrate (IAEA-N3) and the isotopic nitrate reference material United States Geological Survey 34 (USGS-34),
286 with respective $\delta^{15}\text{N}$ vs. air of 4.7 ‰ and -1.8 ‰ vs. air (International Atomic Energy Agency, 1995), and
287 respective $\delta^{18}\text{O}$ of 25.61 ‰ and -27.9 ‰ vs. Vienna Standard Mean Ocean Water (VSMOW; Gonfiantini, 1995;
288 Böhlke et al., 2003). To account for bacterial blanks and source linearity, nitrate concentrations of the standard
289 material – diluted in N-free seawater for aqueous seawater samples and air-equilibrated milli-Q water for
290 skeleton matrix samples – were matched to those of samples within batch analyses, and additional bacterial
291 blanks were also measured (Weigand et al., 2016; Zhou et al., 2022). Replicate measurements ($n \geq 2$) of all
292 samples yielded an average analytical precision (± 1 SD) of 0.3‰ for both $\delta^{15}\text{N}$ and $\delta^{18}\text{O}$.

293

294 2.7. N turnover model

295 We estimate values of the trophic $\delta^{15}\text{N}$ offset for *B. elegans*, ϵ , and the rate of isotopic turnover by fitting
296 the data from our trophic isotope experiment to a nonlinear least-squares regression model corresponding to the
297 isotope mixing relationship shown in Equation 1 below. Equation 1 treats the coral tissue as a single reservoir of
298 N with some initial isotope composition that is evolving to reflect the new diet as a function of time (after Cerling
299 et al. 2007; Ayliffe et al. 2004).

$$300 \quad \delta^{15}\text{N}(t) = [\delta^{15}\text{N}_{t=0} - \delta^{15}\text{N}_{\text{diet}} + \epsilon] \cdot e^{-\lambda t} + \delta^{15}\text{N}_{\text{diet}} + \epsilon. \quad \text{Equation 1}$$

301 The term $\delta^{15}\text{N}_{t=0}$ is the value of the bulk coral tissue at the onset of the experiment, $\delta^{15}\text{N}_{\text{diet}}$ is that of the corals'
302 new *Artemia* diet (i.e. what it is fed during the experiment), t is the number of days since the start of the
303 experiment, ϵ is the difference between the $\delta^{15}\text{N}$ of the diet and tissue at equilibrium (i.e. once the isotopic
304 composition of inputs to the system equals the isotope composition of outputs), and λ describes the specific rate
305 at which new N is incorporated into the coral tissue (days^{-1}). We use this model to calculate the e-folding time of

306 the system, which is defined as $1/\lambda$ (days) and represents the time at which ~63% of the original N reservoir in
307 coral tissue has been replaced with new N from the experimental coral diet.

308

309 3. Results

310 3.1 Trophic isotope effect

311 At the onset of the culture experiment, the soft tissue among all experimental corals had a $\delta^{15}\text{N}$ of 11.7 ± 0.5
312 ‰. Over the course of the experiment, the $\delta^{15}\text{N}$ of the tissue increased or decreased in respective treatments
313 depending on the $\delta^{15}\text{N}$ of their *Artemia* diet (Figure 3); the tissue $\delta^{15}\text{N}$ increased in corals fed diets with $\delta^{15}\text{N}$
314 values of 17.0, 13.8, and 9.9 ‰, whereas the tissue $\delta^{15}\text{N}$ decreased for the diet of 6.4 ‰. The $\delta^{15}\text{N}$ of soft tissue
315 in all groups trended towards an asymptotic offset relative to the diet $\delta^{15}\text{N}$, as expected for an approach to a new
316 equilibrium. However, at day 530, at the end of the experiment, it appeared as though the coral tissue $\delta^{15}\text{N}$ had
317 not yet reached a constant offset value, suggesting that the coral tissue had not yet reached an equilibrium with

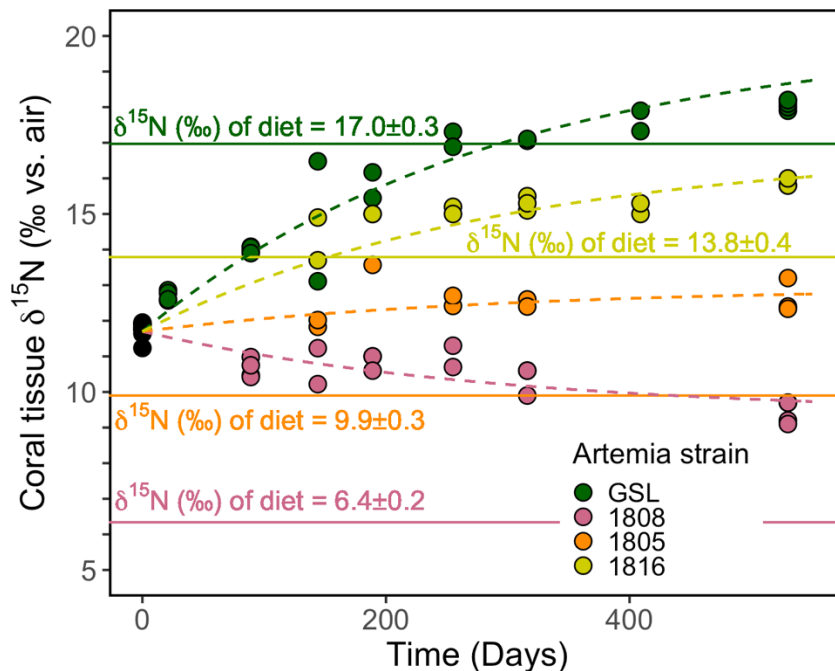


Figure 3. Evolution of the coral soft tissue $\delta^{15}\text{N}$ in response to diet $\delta^{15}\text{N}$. Colors correspond to the respective *Artemia* strains. Dashed lines are the model output of our simultaneous nonlinear least squares regression fits to the data using Equation 1. Solid lines mark the diet $\delta^{15}\text{N} \pm \sigma$. The mean analytical error on tissue $\delta^{15}\text{N}$ analyses was ± 0.2 ‰.

318 the new diet. Specifically, at the end of the experiment, the coral tissue of the treatment groups reached $\delta^{15}\text{N}$
319 values of $9.4 \pm 0.3\text{‰}$, $12.6 \pm 0.5\text{‰}$, $15.9 \pm 0.1 \text{‰}$, and $18.1 \pm 0.1 \text{‰}$ for groups fed the lowest to highest *Artemia*
320 $\delta^{15}\text{N}$ values, respectively. The difference between coral soft tissue and diet $\delta^{15}\text{N}$ ranged from a minimum of $1.0 \pm$
321 0.1‰ to a maximum of $3.0 \pm 0.3\text{‰}$ across the different experimental groups at day 530 (Figure 3).

322 Despite the fact that coral tissue had not yet reached an equilibrium with the new coral diet at the end of our
323 experiment, we are able to estimate values of the trophic $\delta^{15}\text{N}$ offset for *B. elegans*, ϵ , and the rate of isotopic
324 turnover by fitting the data from our trophic isotope experiment to the nonlinear least-squares regression model
325 given Equation 1 in Section 2.7. To more confidently calculate ϵ and λ for each individual experimental group,
326 we generate 4 equations, (one for each experimental group of the form given in Eq. 1 but with different values of
327 $\delta^{15}\text{N}_{\text{diet}}$) and fit them simultaneously using least-squares regression. From this fit, we are able to obtain estimates
328 for both ϵ and λ in *B. elegans*. An inherent assumption of this approach is that all experimental groups have the
329 same e-folding time and the same trophic isotope effect. We note here that we refer to the e-folding time as the
330 ‘turnover rate’ of N in corals throughout the rest of this text (e.g., Tanaka et al. 2018). Our model fit yielded a
331 trophic isotope effect, ϵ , of 3.0‰ with a standard error of 0.1‰ between coral tissue and diet. The turnover rate
332 of N (i.e. e-folding time, $1/\lambda$) was 291 days with a standard error of 15 days. The four individual model equations
333 generated by our nonlinear least squares regression are presented as the dashed lines in Figure 3.

334 3.2 Effect of starvation

335 At the onset of the starvation trial, the coral tissue had an average $\delta^{15}\text{N}$ of $11.5 \pm 0.1 \text{‰}$. At the end of the
336 522-day experiment, the starved group (N=15 coral individuals) had an average $\delta^{15}\text{N}$ of $12.4 \pm 0.4 \text{‰}$ and the
337 frequently fed group (N=15) with a $\delta^{15}\text{N}$ of $12.7 \pm 0.1 \text{‰}$ (Figure 4). The starved group was $+2.5 \pm 0.4 \text{‰}$

338 compared to its diet, statistically indistinguishable from that of the frequently fed group of $+2.8 \pm 0.1$ ‰ higher
339 than the diet (p-value = 0.059, pairwise t-test).

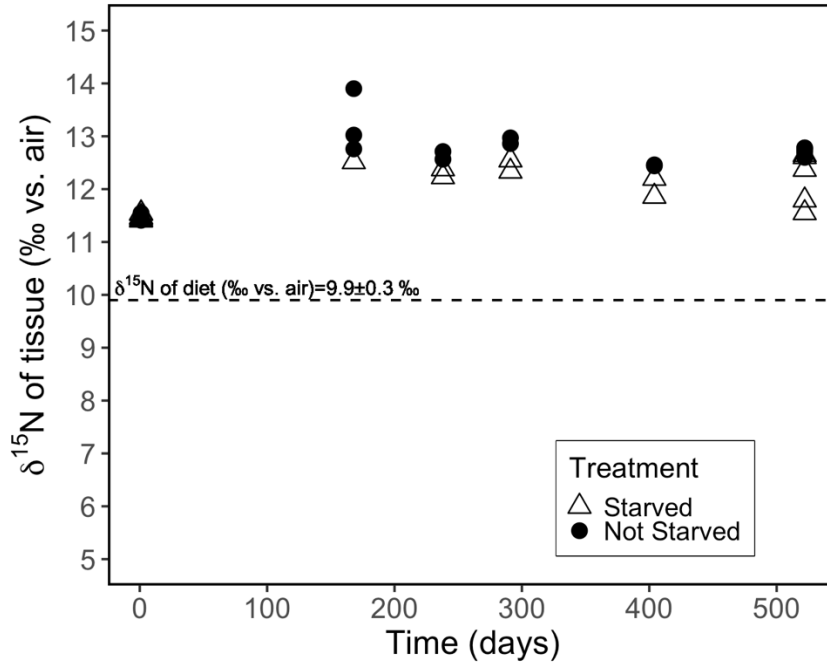


Figure 4. Evolution of the $\delta^{15}\text{N}$ of individual coral polyps fed *Artemia* nauplii ($\delta^{15}\text{N}$ 9.9 ‰) twice weekly (not starved) vs. every two weeks (starved). The analytical error associated with individual tissue $\delta^{15}\text{N}$ measurements was ± 0.2 ‰.

340 3.3 $\delta^{15}\text{N}$ comparison of field specimen polyp tissue and skeleton

341 The $\delta^{15}\text{N}$ of the soft tissue from individual *B. elegans* specimens collected live near Friday Harbor ranged
342 between 11.2 to 13.1 ‰, averaging 12.0 ± 0.6 ‰ (Figure 5a). The soft tissue $\delta^{15}\text{N}$ differed among coral groups
343 collected during different sampling campaigns, with higher values in spring (March 2019 and April 2021)
344 compared to summer and fall (June 2019, September and November 2020; ANOVA $F(4) = 40.39$; p-value ≤ 0.01 ,
345 post-hoc pairwise t-test; p-value < 0.05). The average $\delta^{15}\text{N}$ of corresponding skeletal tissue was 13.5 ± 0.7 ‰ and
346 did not differ discernibly among sampling campaigns (ANOVA $F(2) = 0.916$; p-value = 0.431). The average

347 difference between skeleton and soft tissue $\delta^{15}\text{N}$ ($\Delta\delta^{15}\text{N}$) among coral individuals for which both soft tissue and
348 skeleton was measured was 1.2 ± 0.6 ‰ (Figure 5b).

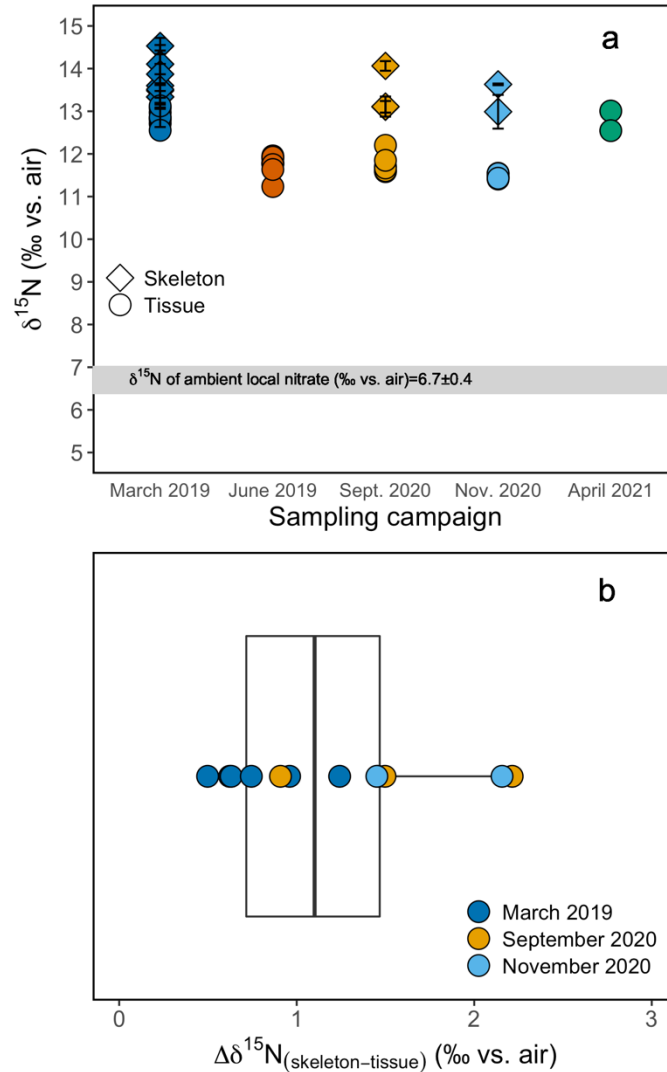


Figure 5. (a) Tissue and skeleton $\delta^{15}\text{N}$ measurements from *B. elegans* individuals collected during different sampling campaigns. Errors on skeleton data are based on replicate analyses of samples from individual polyps. (b) Boxplot of the difference between tissue and skeleton of individual *B. elegans* corals. The boxplot shows the mean, first and third quartile, maxima, and minima. Individual data points are overlaid on the plot. Colors correspond to respective sampling campaigns.

349 3.4 Regional hydrography and N isotope ratios of nitrate and plankton material

350 Hydrographic profiles recorded at stations near Friday Harbor in August 2021 showed characteristic density
351 structures that were sensitive to tidal phase (Figure 6 a,b; Banas et al. 1999). Profiles collected during flood tide

352 (collected between 11:40 and 14:20 on August 2, 2021) were relatively well-mixed (salinity 30, temperature
 353 11.8°C), with fresher and warmer water restricted to the near surface (≤ 5 m), whereas ebb-tide profiles (collected
 354 at 9:00 on August 2, 2023) showed a progressive decrease in salinity from 30 to 27 and a corresponding increase
 355 in temperature from 11.8°C at 35 m to 14.5°C at the surface.

356 Nitrate concentrations were nearly uniform with depth during flood tide ($\sim 20 \mu\text{mol L}^{-1}$), decreasing slightly at
 357 5 m, whereas during ebb tide nitrate concentrations decreased progressively from 20 to $10 \mu\text{mol L}^{-1}$ between 30
 358 and 10 m (Figure 6c). Nitrate concentrations in samples collected during the other sampling campaigns ranged
 359 from 12 to $32 \mu\text{mol L}^{-1}$, and appeared generally higher at stations visited during the September and November
 360 2020 campaigns compared to those in April and August 2021 (Figure S6).

361 Depth profiles collected in August 2021 revealed uniform nitrate $\delta^{15}\text{N}$ values of $\sim 7 \text{‰}$ at 30 m among
 362 profiles. In well-mixed profiles, nitrate $\delta^{15}\text{N}$ increased slightly to 7.5 ‰ above 10 m. In stratified profile, nitrate
 363 $\delta^{15}\text{N}$ increased progressively to 8.2 ‰ at 10 m (Figure 6d). Among all sampling campaigns, the $\delta^{15}\text{N}$ of nitrate
 364 ranged from 6.1 ‰ to 8.2 ‰, with median values of $6.8 \pm 0.4 \text{‰}$ (Figure 7a). The relationship between nitrate
 365 $\delta^{15}\text{N}$ and nitrate concentration in August 2021 was fit to a closed-system Rayleigh distillation model (Mariotti et
 366 al. 1981), suggesting a nitrate assimilation isotope effect of $1.5 \pm 0.1 \text{‰}$ (Figure 8).

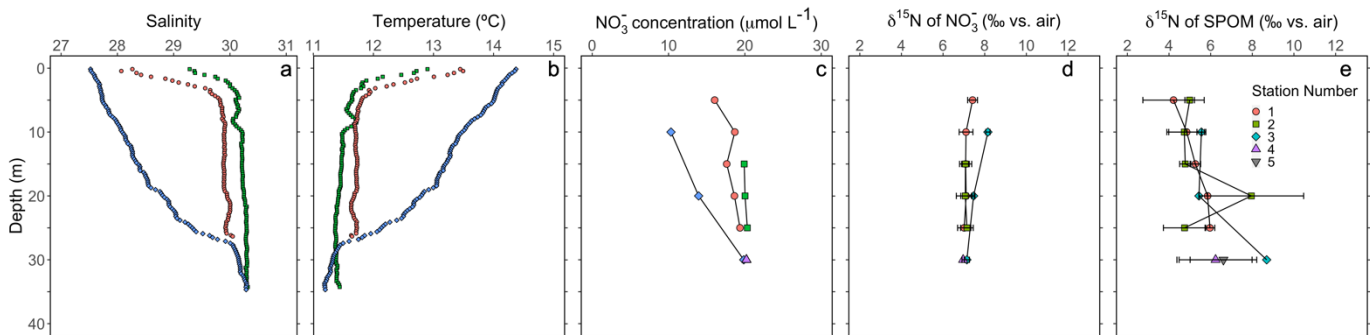


Figure 6. Depth profiles during the August 2021 sampling campaign of (a) salinity, (b) temperature, (c) nitrate concentration, (d) the $\delta^{15}\text{N}$ of nitrate for analytical replicates and (e) the $\delta^{15}\text{N}$ of SPOM of replicate samples ($n \geq 2$). Green and red symbols correspond to flood tide (collected between 11:00am and 2:00pm on August 2, 2021), blue symbols correspond to ebb tide (collected at 9:00am on August 3, 2021).

367 The $\delta^{15}\text{N}$ of SPOM collected at depths above 35 m near Friday Harbor during the different sampling
 368 campaigns ranged from 1.6 to 11.7 ‰, averaging $5.7 \pm 1.7 \text{‰}$ (Figure 7b). Values were lowest for the four
 369 samples collected in April ($4.4 \pm 0.4 \text{‰}$), and highest for the four samples collected in September and November
 370 ($6.2 \pm 2.6 \text{‰}$), although these trends may be an artifact of the low data density in April ($n = 4$) and Sept./Nov. (n
 371 $= 5$) relative to August 2021 ($n = 29$), at which time the observed range of $\delta^{15}\text{N}$ subsumed that in the other two

372 campaigns. Values did not differ coherently with depth in August 2021, although any potential depth structure
373 was obscured by the large variability among sample replicates (Figure 6e).

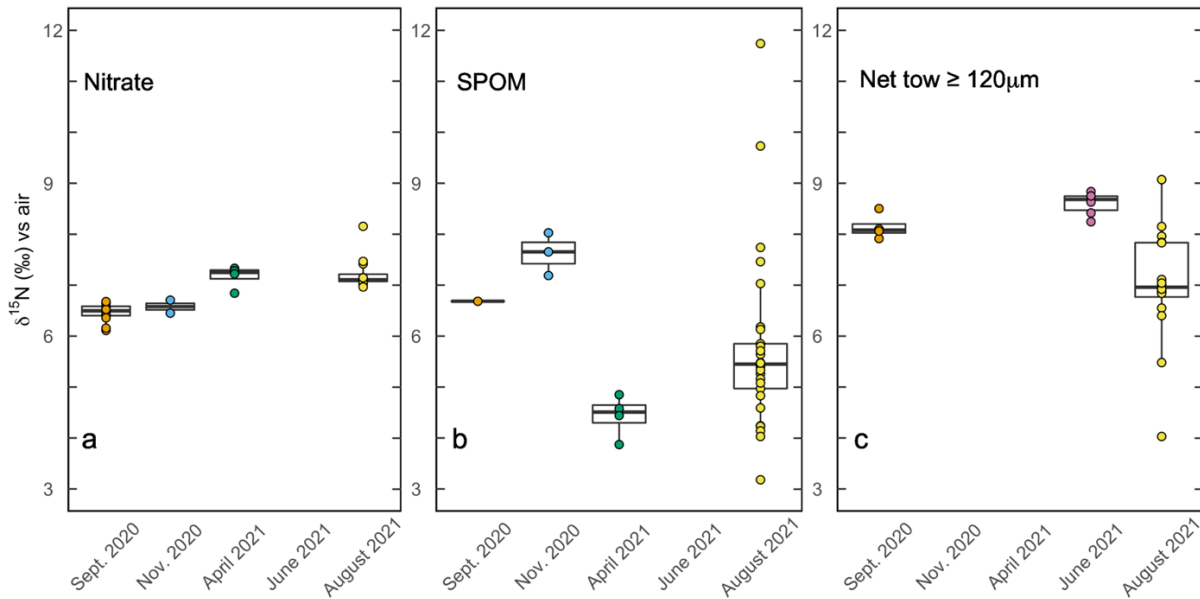


Figure 7. Boxplots of aqueous and particulate N pools at respective sampling times. (a) The $\delta^{15}\text{N}$ of nitrate from samples above 30 m collected during respective sampling campaigns. (b) The $\delta^{15}\text{N}$ of suspended particulate organic matter (SPOM) at sites near Friday Harbor during respective sampling campaigns. (c) The $\delta^{15}\text{N}$ of net tows ($\geq 120 \mu\text{m}$ mesh size) conducted during respective sampling campaigns.

374 The $\delta^{15}\text{N}$ of material collected in net tows ($120 \mu\text{m}$ mesh size) during sampling campaigns in September 2020,
375 and June 2021 ranged between 7.9 to 8.8 ‰ (Figure 7c). Material collected in net tows of $80 \mu\text{m}$ and $150 \mu\text{m}$
376 mesh size in August 2021 and separated by size class post-collection revealed a coherent $\delta^{15}\text{N}$ increase with size
377 class (Figure 7c; Figure 9). The $\geq 80 \mu\text{m}$ size class had a mean $\delta^{15}\text{N}$ of $6.0 \pm 0.3 \text{ ‰}$ whereas that $\geq 500 \mu\text{m}$ had an
378 average $\delta^{15}\text{N}$ of $8.0 \pm 0.8 \text{ ‰}$, which was significantly greater than the $\delta^{15}\text{N}$ of the other size classes (ANOVA, p-
379 value < 0.05).

380 4. Discussion

381 This study of *B. elegans* provides novel constraints on the trophic ecology of scleractinian CWCs. Foremost,
382 our observations of *B. elegans* collectively suggest that the relatively large global $\delta^{15}\text{N}$ offset of 8-9 ‰ between
383 CWC skeletal tissue and the $\delta^{15}\text{N}$ of PON exported from the surface ocean is neither explained by a large
384 difference between tissue and skeleton $\delta^{15}\text{N}$, nor by an unusually large trophic isotope effect. Further, controlled

385 feeding experiments yielded direct estimates of the trophic isotope effect and the corresponding N turnover rate
386 of *B. elegans* soft tissue. Examination of soft tissue $\delta^{15}\text{N}$ of wild specimens in relation to regional hydrography
387 and food web components near Friday Harbor leads us to conclude that *B. elegans* feeds predominantly metazoan
388 zooplankton prey, implicating more than one trophic transfer between exported PON and coral soft tissue. We
389 contextualize our findings to existing studies of CWC trophic ecology and discuss the implications of considering
390 a two-level trophic transfer for paleo-reconstructions of ocean N cycling using *B. elegans* and CWCs more
391 generally.

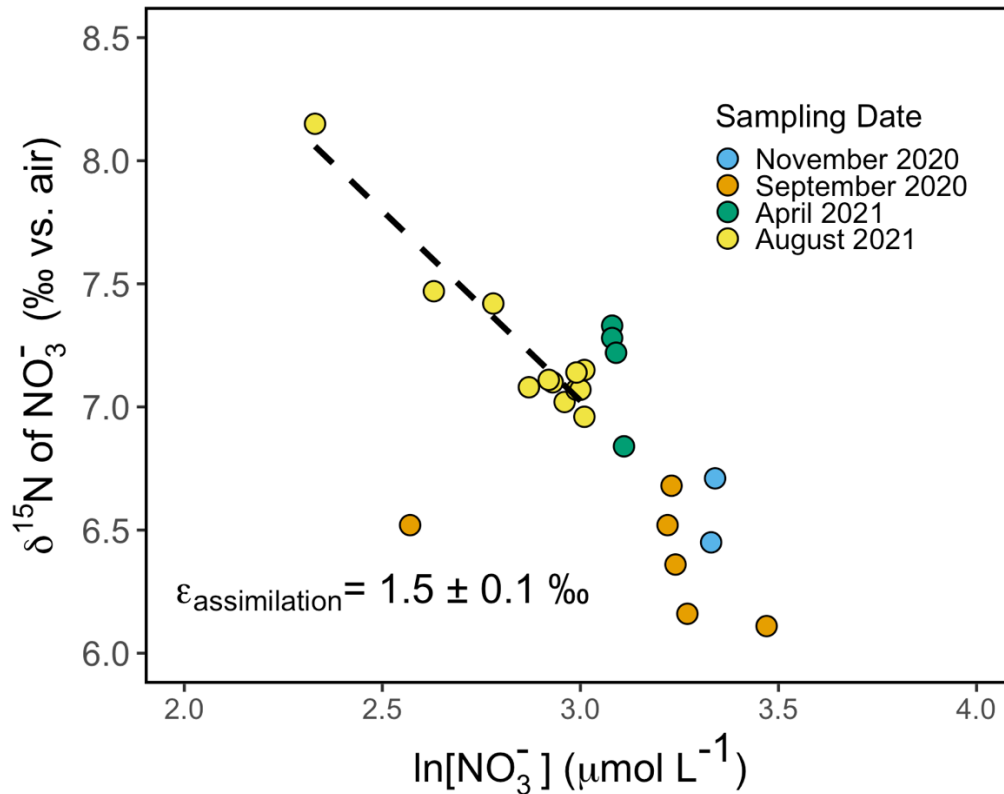


Figure 8. Rayleigh plot of nitrate $\delta^{15}\text{N}$ vs. \ln of nitrate concentration for samples collected from the surface to 40 m around Friday Harbor. The isotope effect of $\sim 1.5 \pm 0.1 \text{ ‰}$ corresponds to the slope of the best fit linear regression line for the August 2021 data, $\delta^{15}N_{\text{NO}_3} = 11.7 - 1.5 \ln [\text{NO}_3^-]$.

392 4.1 Culture experiments revealed a normal trophic isotope effect

393 We investigated whether the large difference in $\delta^{15}\text{N}$ between PON export from the surface and coral
394 skeleton-bound $\delta^{15}\text{N}$ (8-9 ‰) observed by Wang et al. (2014) could arise from an unusually large trophic level
395 offset specific to CWCs. The long-term feeding experiment of *B. elegans* polyps revealed a ‘normal’ trophic

396 isotopic offset between coral tissue and diet of $\epsilon = +3.0 \pm 0.1 \text{ ‰}$. This value conforms to the expected range of
397 $+3.4 \pm 1.1 \text{ ‰}$ for a single trophic level offset in $\delta^{15}\text{N}$ (Minagawa and Wada, 1984).
398

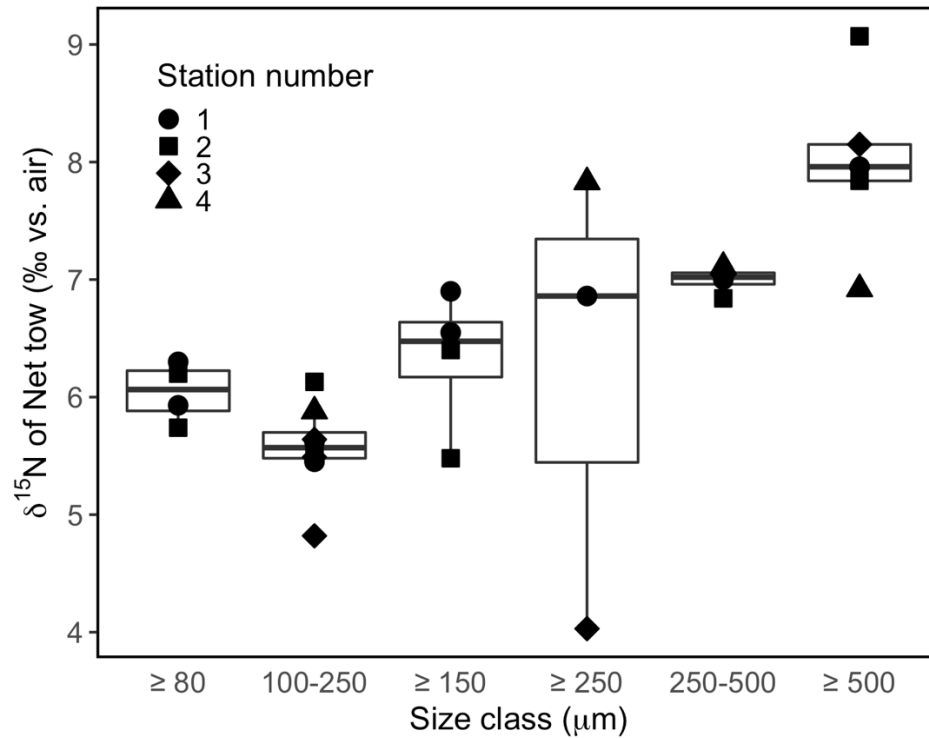


Figure 9. Boxplots of net tow material collected above 30 m in August 2021, separated by size class.

399

400 To support the above conclusion, we assess the assumptions inherent to the isotope mixing model (Eq. 1)
401 used to derive ϵ and the corresponding nitrogen turnover rate from our culture data. First, the model only
402 accounts for the turnover of a single pool of N, requiring the assumption that all N in the coral polyp tissues
403 equilibrate at the same rate. This notion is unlikely to be wholly accurate, as fluxes of N may vary among tissue
404 types. However, given the relatively low resolution of our sampling over the course of the culture experiments
405 (necessary due to constraints on numbers of total samples) we are unable to extend our model to one with
406 multiple pools (*e.g.* as in Ayliffe et al. 2004). As soft tissues of individual coral polyps were homogenized, we
407 suggest that the $\delta^{15}\text{N}$ values and corresponding estimate of ϵ thus represent the average of soft tissues with
408 potentially different turnover rates. The estimates of ϵ and N turnover rate further rely on the assumption that the

409 nutritional quality of the respective diets among treatments was equivalent, as trophic isotope effects can be
410 sensitive to food type. Diets low in protein can be associated with greater ϵ values due to internal recycling of
411 nitrogen (Adams and Sterner, 2000; Webb et al., 1998). For instance, locusts fed a low protein diet were enriched
412 5.1 ‰ from their diet, compared to 2.3‰ for those fed a high protein diet (Webb et al., 1998). Conversely, a
413 compilation of studies of various metazoan consumers raised on controlled diets suggests that high protein diets
414 generally result in higher trophic isotope effects (~3.3 ‰) compared to more herbivorous diets (~2.2 ‰), a
415 dynamic ascribed to higher rates of N excretion to assimilation in consumers fed high protein diets (McCutchan
416 Jr et al., 2003). As noted in Table S3 and in Section 2.3.1, our *Artemia* prey had similar C:N ratios among
417 treatments, in line with our model treatment. Finally, our model assumes that N turnover was dominated by
418 metabolic tissue replacement, rather than net growth, consistent with the observation that adult *B. elegans* growth
419 is slow (Gerrodette 1981).

420 Equation 1 could be invalidated if the corals can access nutritional N sources other than N in *Artemia*, given
421 that the model assumes that *Artemia* are the only source of N to corals in our experiment. Biological N₂ fixation
422 and chemoautotrophy have been detected in association with CWC holobionts, providing some N nutrition to the
423 corals (Middelburg et al., 2016). Our trophic isotope effect estimate was in the range expected for a single trophic
424 transfer, arguably suggesting that N₂ fixation, if occurring, was not a substantial contribution to the corals'
425 nutrition; it would otherwise result in a lower value of ϵ given a $\delta^{15}\text{N}$ contribution of -1 to 0 ‰ (Carpenter et al.
426 1997). That the trophic isotope effect of the poorly fed corals did not differ from that of corals that were well-fed
427 also argues for no sources of N additional to the *Artemia*, as starved corals would presumably increase their
428 reliance on said source. In a related vein, N recycling between the *B. elegans* specimens and potential microbial
429 symbionts (e.g. Middelburg et al. 2016) could also dampen the trophic isotope effect relative to the *Artemia* prey
430 and yield an over-estimate of soft tissue turnover rate for N. The normal trophic isotope effect indicated here
431 suggests a modest role of N retention and recycling by microbial symbionts, in contrast to tropical symbiotic
432 corals wherein bacterial symbionts promote substantial N retention and recycling, and consequently lower trophic
433 isotope effects (Tanaka et al. 2018). Finally, the validity of our estimates could be sensitive to differences in
434 feeding rates, which can influence the rate of N turnover of tissues (Martínez del Río and Carleton, 2012; Rangel
435 et al., 2019). Corals were fed at identical times among treatments, at a relatively high feeding rate (Crook et al.,
436 2013). However, given the limited number of studies on feeding in *B. elegans*, it is difficult to compare our
437 feeding strategy and that of this species' natural environment. Overall, we consider that the mixing model

438 described by Equation 1 is appropriate to derive the first-order trophic isotope effect and turnover rate of *B.*
439 *elegans*.

440 Changes in metabolism due to underfeeding or prolonged fasting have the potential to increase trophic-level
441 isotope offsets due to increased protein metabolism (Adams and Sterner, 2000). For instance, extensive amino
442 acid recycling in overwintered adult insect larvae was cited to explain trophic isotope effects upward of 10%
443 (Scrimgeour et al., 1995). A meta-analysis on the effects of starvation on consumer $\delta^{15}\text{N}$ revealed that starvation
444 generally led to increased organism $\delta^{15}\text{N}$ by an average of 0.5 ‰, up to 4.3 ‰ (Doi et al., 2017). This dynamic
445 was documented for the tropical symbiotic coral *Stylophora phistillata*, where heterotrophically starved corals
446 were enriched in $\delta^{15}\text{N}$ by ~0.5 ‰ compared to frequently fed corals (Reynaud et al., 2009). The trophic isotope
447 offset of *B. elegans* soft tissue relative to its diet, ϵ , was not discernibly influenced by near starvation; that of
448 corals fed once every other week was similar to that of corals fed twice a week – in spite of visible signs of stress
449 among the former, including relatively more sluggish feeding (Figure S7) and thinner soft tissue (data not
450 shown). Deep sea coral reefs are often highly productive environments with high levels of biodiversity,
451 commensurate with a relatively high food supply (Duineveld et al., 2007; 2004; Genin et al., 1986; Roberts et al.,
452 2006; Soetaert et al., 2016; Thiem et al., 2006; Cathalot et al. 2015). Nevertheless, periodicity and spatial
453 heterogeneity in the food supply of CWC reefs implicate periods of lower food density (e.g., Duineveld et al.
454 2007). High currents, downwelling and/or vertically migrating zooplankton temporally boost the export of
455 surface organic matter to the seabed, creating ‘feast’ conditions, interspersed with ‘famine’ periods during the
456 non-productive season (Maier et al. 2023). Regardless, our trials suggest that starvation, if pertinent to CWC
457 communities, does not result in greater-than-expected trophic isotope offsets, at least for *B. elegans*.

458 4.2 Turnover rate for *B. elegans*

459 We report the first estimate of the nitrogen turnover for a non-symbiotic cold-water coral of 291 ± 15 days
460 for *B. elegans* soft tissue. This value falls within the range of existing estimates for tropical symbiotic corals.
461 Pulse-chase experiments with ^{15}N -nitrate conducted with fragments of the tropical symbiotic coral *Porites*
462 *cylindrica* yielded a N turnover time of 370 days, and of 210 days for the tropical symbiotic coral *Acropora*
463 *pulchra* (Tanaka et al. 2006; 2018). These relatively long turnover times are attributed to the recycling and
464 retention of N within the coral-symbiont system in nutrient-deplete ecosystems. In comparison, the corresponding
465 carbon turnover in *A. pulchra* was 18 days – compared to 210 days for N – because the system is ultimately N
466 limited (Tanaka et al., 2006). Tanaka et al. (2018) inferred that the N turnover in *P. cylindrica* would be
467 substantially faster than 370 days without symbionts, on the order of 56 days based on estimates of polyp-specific

468 N uptake rates. Nevertheless, the N turnover estimated for the tropical symbiotic coral *Porites lutea* was notably
469 shorter than *A. pulchra* and *P. cylindrica*, on the order of 87 days (Rangel et al., 2019), implicating different N
470 nutritional strategies among symbiotic coral groups and/or ecosystems. The N turnover for *B. elegans* estimated
471 here is of the same order as but still longer than that for tropical symbiotic corals suggesting that cold-water
472 species have lower metabolic and growth rates compared to tropical symbiotic species, although efficient N
473 recycling has also been documented previously in cold-water corals (Middelburg et al. 2016). The slower
474 turnover of CWCs relative to their symbiotic tropical counterparts may reflect the lower temperatures of the
475 former's habitats (Miller, 1995; Thomas and Crowther 2015).

476 Constraints on N turnover also allow for calibration of the temporal resolution that is achievable with the
477 CWCs $\delta^{15}\text{N}$ proxy for marine N cycling. Corals are constantly accreting skeleton, such that coral proxies have the
478 potential to provide annual resolution (e.g., Adkins et al. 2004). In theory, a rapid N turnover in CWC could
479 record seasonal changes in regional N dynamics. A turnover time of 291 ± 15 days for N in *B. elegans* soft tissue,
480 however, signifies that the $\delta^{15}\text{N}$ of coral skeleton is unlikely to provide a faithful record of seasonal differences in
481 the $\delta^{15}\text{N}$ of the coral diet. Moreover, the turnover of the pool of N that sources the skeletal tissue may be different
482 from that of bulk tissue, and thus decoupled from the soft tissue turnover rate. We suggest that CWCs can likely
483 record changes in their diet on annual or longer timescales, compatible with the ability to date CWC with
484 subdecadal resolution (Adkins et al. 2004).

485 4.3 Soft tissue vs. skeleton $\delta^{15}\text{N}$

486 A large biosynthetic $\delta^{15}\text{N}$ offset between the coral soft tissue and its skeleton could conceivably account for a
487 large $\delta^{15}\text{N}$ offset between coral skeleton-bound organic matter and N of export that is not explained by single
488 trophic level enrichment of ~ 3 ‰. However, the mean difference between soft tissue and skeleton-bound $\delta^{15}\text{N}$
489 among *B. elegans* specimens collected at Friday Harbor was relatively modest, on the order of +1.2 ‰, ranging
490 between +0.5 and +2.2 ‰. The observed range was dictated primarily by the variability in the $\delta^{15}\text{N}$ of the coral
491 soft tissue, as skeleton-associated $\delta^{15}\text{N}$ values were relatively invariant among specimens sampled from different
492 locations and field seasons – likely due to the fact that the amount of skeleton analyzed represented multiple
493 years of growth. The amount of skeleton-bound organic N is small relative to aragonite mass (2-5 $\mu\text{mol N per g}$
494 of skeleton in our samples), such that homogenization of 50-100 mg aragonite fragments may alias seasonally-
495 driven variability in skeletal $\delta^{15}\text{N}$. Soft tissue values in spring were ~ 1.5 ‰ higher than in summer and fall, such
496 that they appeared to record seasonal changes in diet (Figure 5a). In this regard, the asymptotic nature of the two
497 end-member isotope mixing model (Eq. 1) renders *B. elegans*'s soft tissue sensitive to seasonal changes in prey

498 $\delta^{15}\text{N}$, but not likely to reach isotopic equilibrium on seasonal timescales - given an N turnover of ~ 291 days, as
499 discussed above. Seasonal variations in the $\delta^{15}\text{N}$ of the food source of *B. elegans* near Friday Harbor could arise
500 from corresponding differences in the $\delta^{15}\text{N}$ of nitrate entrained to the surface driven by seasonal hydrographic
501 variability around San Juan archipelago, in the extent of surface nitrate consumption, in food web structure, or
502 from some combination of these. The data density among all but the August 2021 sampling campaign is too
503 sparse to be conclusive in this regard. Otherwise, the observed differences in soft tissue $\delta^{15}\text{N}$ may result from
504 spatial heterogeneity in food source $\delta^{15}\text{N}$ among the different collection sites visited for respective campaigns at
505 Friday Harbor.

506 As documented here for *B. elegans*, the $\delta^{15}\text{N}$ difference between coral tissue and skeleton appears to be
507 modest among various scleractinian coral species. Specimens of the symbiotic tropical coral *Porites lutea* showed
508 a $\delta^{15}\text{N}$ offset of +1.1 ‰ between skeleton and soft tissue, whereas the symbiotic tropical coral *Favia stelligera*
509 revealed an insignificant offset of -0.1 ‰ (Erler et al., 2015). Similarly, no offset was observed for proteinaceous
510 cold-water corals of the genus *Lepidisis* collected off Tasmania (Sherwood et al., 2009), whereas an offset of -1.9
511 ± 0.8 ‰, was reported for cold-water proteinaceous corals of the genus *Primnoa* from the Gulf of Alaska,
512 *Isadella* from the Central California Margin, and *Kulamanamana* from the North Pacific Subtropical Gyre
513 (McMahon et al., 2018). Conversely, a study of numerous species of both symbiotic and non-symbiotic corals
514 reported a +4 ‰ offset between the skeletal organic matrix and soft tissue among the non-symbiotic corals
515 specifically, but no difference among the symbiotic corals (Muscatine et al., 2005), suggesting that biosynthetic
516 offsets may occur for certain CWC species or conditions.

517 4.4 Implications for components of CWC diet

518 Cold water corals are considered opportunistic feeders, ingesting whatever is available in the water column
519 (Mortensen, 2001; Freiwald, 2002; Duineveld et al. 2004; 2007; Kiriakoulakis et al. 2005; Carlier et al. 2009;
520 Dodds et al. 2009; van Oevelen et al. 2009). They are reported to feed on zooplankton (Kiriakoulakis et al., 2005;
521 Naumann et al., 2011), including microzooplankton (Houlbrèque et al. 2004), on phytoplankton and
522 phytodetritus, including the bacterial fraction of phytodetritus (Maier et al., 2020; Houlbrèque et al. 2004),
523 dissolved organic matter (Mueller et al., 2014; Ferrier 1991, Al-Moghrabi et al. 1993; Hoegh-Guldberg &
524 Williamson 1999; Houlbrèque et al. 2004; Grover et al. 2008), and the CWC holobiont has been observed to
525 display biological N_2 fixation and chemoautotrophy (Middelburg et al. 2016). While it is clear that corals may be
526 able to consume a variety of components within the food web, the soft tissue $\delta^{15}\text{N}$ of *B. elegans* specimens
527 collected at Friday Harbor averaged 12.0 ‰, signifying that they fed on material with a $\delta^{15}\text{N}$ of approximately

528 9.0 ‰ – accounting for a normal trophic offset relative to their diet (3 ‰) confirmed by our culture experiment
529 results. Here, we seek to determine the primary nutrition source for *B. elegans* at Friday Harbor by comparing the
530 $\delta^{15}\text{N}$ of these corals' expected diet with measured $\delta^{15}\text{N}$ of different food web components including SPOM and
531 net tow material.

532 We first explore whether the SPOM fraction of the food web was the dominant component of *B. elegans*' diet
533 at Friday Harbor. SPOM is operationally defined as the particulate material retained onto glass fiber filters (GF/F,
534 0.7 μm nominal pore size) from filtered aqueous samples. At the ocean surface, including at the stations near
535 Friday Harbor, SPOM is generally dominated by phytoplankton material. At the ocean subsurface, below the
536 euphotic zone, SPOM derives from organic material exiting the ocean surface, but is considered a distinct pool
537 from the ballasted sinking PON collected in sediment traps. The $\delta^{15}\text{N}$ of SPOM typically increases with depth,
538 with the steepest gradient across the 100-300 m depth interval, reaching upwards of ~4-5 ‰ in the ocean
539 subsurface, which are higher values than the corresponding sinking particles at abyssal depths due to recycling
540 and remineralization (Altabet, 1988; Casciotti et al., 2008; Saino and Hattori, 1987). Wang et al. (2014) reasoned
541 that because the $\delta^{15}\text{N}$ of SPOM is approximately one trophic level lower than that of the N preserved in skeletons of
542 the deep-dwelling (deeper than ~ 500 m) CWC *Desmophyllum dianthus*, and because suspended particles are the
543 most abundant form of small particles in the deep ocean, cold-water corals must feed predominantly on SPOM.
544 However, SPOM collected in the upper 30 meters near Friday Harbor was 5.7 ± 1.7 ‰, which is ~ 6 ‰ lower
545 than *B. elegans* soft tissue, a difference greater than expected for a single trophic level. Thus, the SPOM at Friday
546 Harbor was evidently not the predominant food source for *B. elegans* growing in this depth interval.

547 Additionally, it has been suggested that CWCs can assimilate dissolved organic nitrogen (DON) (Gori et al.,
548 2014). We do not have $\delta^{15}\text{N}$ DON measurements from our field study. However, we do not expect the potential
549 assimilation of DON to explain the elevated $\delta^{15}\text{N}$ of organic tissue that was observed. There are two components
550 of marine DON, refractory and labile (Bronk et al. 2002), which have different $\delta^{15}\text{N}$ (Knapp et al. 2018). At
551 Friday Harbor, we don't know the partitioning of the $\delta^{15}\text{N}$ between these pools, but even if we did, the labile
552 fraction (which would presumably be the pool available to corals) is expected to converge on the $\delta^{15}\text{N}$ value of
553 SPOM (Bronk et al., 2002, Sigman and Fripiat 2019 their Fig. 4; Knapp et al., 2018, Zhang et al., 2020), given
554 that the most recently produced DON is generally most labile. As a result, consumption of DON would not
555 explain the high $\delta^{15}\text{N}$ of coral organic tissue.

556 Instead, we suggest that the relatively high $\delta^{15}\text{N}$ of ~ 12 ‰ of *B. elegans* soft tissue at Friday Harbor results
557 from these corals deriving nutrition predominantly from larger metazoan zooplankton. Indeed, this is supported
558 by a comparison of the $\delta^{15}\text{N}$ coral tissue and the $\delta^{15}\text{N}$ of the largest size class of net tow material ($\geq 500 \mu\text{m}$) of

559 8.0 ± 0.8 ‰. This is the only component of the organic matter nitrogen budget that is offset from the coral tissue
560 by ~ 3.5 ‰, consistent with one trophic level transfer. Additionally, the net tow material had a molar C:N ratio of
561 4.4 ± 0.6, compared to 6.5 ± 2.2 for the SPOM (Figure S8), suggesting a dietary preference for metazoan
562 zooplankton would provide higher protein content and nutritional density for these corals (Adams and Sterner,
563 2000).

564 Despite evidence for zooplankton as the main dietary source for *B. elegans* at Friday Harbor, we
565 acknowledge that this feeding strategy may not apply for corals of other species living in habitats that are
566 hundreds to thousands of meters deep. As pointed out in a recent review (Maier et al. 2023), the presence of
567 CWC reefs in the food-limited deep ocean appears paradoxical, and it is not likely that the food available to
568 corals at Friday Harbor looks identical to food available to corals living at >1000 m water depth. Indeed, Maier et
569 al. 2023 suggest that the biodiversity and productivity of CWC reefs in the deep sea are supported by a number of
570 processes such as CWC's ability to consume a range of dietary components (DOM, bacterioplankton, inorganic
571 resources such and inorganic C and ammonium), efficient resource recycling, and their ability to align their
572 feeding strategies and growth with fluctuations in food availability. While we cannot speculate about the flux of
573 DOM to corals living at >1000m depth, the $\delta^{15}\text{N}$ of deep DOM has a uniform value of ~5 ‰, which cannot
574 explain the high $\delta^{15}\text{N}$ of CWCs (see Sigman and Fripiat, 2019).

575 Maier et al. (2023) and references therein highlight that most deep CWC reefs occur in regions with higher-
576 than-average annual primary productivity, indicating that these CWC reefs are sustained by inputs of high energy
577 to the system, where there is also evidence for the presence of vertically migrating zooplankton. The vertically
578 migrating zooplankton have been found near both relatively shallow (<200 m, Duineveld et al. 2007, Garcia-
579 Herrera et al., 2022) and deep (~1000 m, e.g. Carlier et al. 2009) CWC reefs. Moreover, there are a number of
580 other independent studies that reveal a single trophic level offset between the $\delta^{15}\text{N}$ of zooplankton prey and the
581 $\delta^{15}\text{N}$ soft tissue of asymbiotic scleractinian corals at specific sites (Duineveld et al., 2004, Sherwood et al. 2005;
582 2008; 2009; Carlier et al., 2009; Hill et al., 2014; Maier et al., 2020). Given the 'normal' trophic level offset
583 reported for CWCs in our laboratory culture experiment, these published observations underscore that
584 zooplankton could be a dominant dietary component of corals other than *B. elegans* as well. Additional evidence
585 from lipid biomarkers corroborates the assertion that deep-dwelling CWC species such *Lophelia pertusa*
586 (recently re-classified as *Desmophyllum pertusum*) and *Madrepora oculata* feed predominantly on metazoan
587 zooplankton (Dodds et al., 2009; Kiriakoulakis et al., 2005; Naumann et al. 2015). Some deep-dwelling CWCs
588 (*Desmophyllum pertusum*, *Madrepora oculata*, *Dendrophyllia cornigera*) exhibit prey preference for larger

589 zooplankton (Da Ros et al. 2022), suggesting that zooplankton prey are an essential component of their diet.
590 Indeed, an exclusive diet of phytodetritus (Maier et al. 2019) and the exclusion of zooplankton from diet
591 (Naumann et al. 2011) led to decreases in coral metabolism. More fundamentally, the shared traits of tentacles
592 and nematocysts are evidence of a predatory life strategy, indicating that zooplankton are an important food
593 source for corals (Lewis and Price, 1975; Sebens et al., 1996). The coral morphology of *B. elegans* and that of
594 other cold water scleractinian corals is consistent with an adaptation for the capture of prey of a commensurate
595 size (Fautin, 2009). Correspondingly, *D. dianthus* is considered to be a generalized zooplankton predator that can
596 prey on medium to large copepods and euphysiids (Höfer et al., 2018). In contrast, gorgonian corals do not
597 capture naturally occurring zooplankton and have a correspondingly low density of nematocysts (Lasker 1981).
598 In summary, while our data cannot directly indicate that all CWCs, including the deep-dwelling ones, derive their
599 primary nutrition from zooplankton, the results of our trophic experiment and field study (when evaluated in the
600 context of the published literature) suggest that it may be important to consider metazooplankton as a significant
601 component of CWC diet, and that CWC $\delta^{15}\text{N}$ is likely to be sensitive to food web dynamics. We discuss the
602 implications of these suggestions further in the sections below.

603 4.5 Does coral-bound $\delta^{15}\text{N}$ reflect surface ocean processes at Friday Harbor?

604 The effectiveness of coral skeleton-bound $\delta^{15}\text{N}$ as an archive to reconstruct past ocean N cycling depends on
605 its ability to record the $\delta^{15}\text{N}$ of the surface PON export. In turn, the $\delta^{15}\text{N}$ imparted to the phytoplankton
606 component of surface particles, from which PON export derives, is highly dependent on surface ocean dynamics
607 that influence the degree of nitrate consumption and associated isotope fractionation. Here, we describe local
608 marine N cycling dynamics in order to evaluate whether coral-bound $\delta^{15}\text{N}$ recorded in the *B. elegans* specimens
609 reflects local surface ocean processes.

610 Given complete assimilation of inorganic N pools, the $\delta^{15}\text{N}$ of phytoplankton material - the dominant
611 component of SPOM at the surface ocean - converges on the $\delta^{15}\text{N}$ of the N sources, new nitrate and recycled N
612 sources (Treibergs et al., 2014; Fawcett et al. 2011). At steady state, the $\delta^{15}\text{N}$ of the sinking PON flux reflects the
613 isotope signature of the nitrate upwelled to the surface (Altabet, 1988). Alternatively, given partial nitrate
614 consumption in the context of a finite pool (Rayleigh dynamic), such as in high-nutrient low-chlorophyll regions
615 and in upwelling systems, the SPOM $\delta^{15}\text{N}$ is fractionated relative to the nitrate $\delta^{15}\text{N}$ as function of the
616 assimilation isotope effect and the extent of nitrate consumption (Sigman et al., 1999). The $\delta^{15}\text{N}$ of the sinking
617 flux then reflects both the $\delta^{15}\text{N}$ of nitrate upwelled to the surface and the degree of nitrate consumption (Altabet

618 and François 1994; François et al. 1997). In this section, we discuss whether coral-bound $\delta^{15}\text{N}$ reflects the $\delta^{15}\text{N}$ of
619 nitrate entrained to the surface.

620 Nitrate assimilation at Friday Harbor appeared to be incomplete, potentially implicating the fractionation of
621 N isotopes between nitrate and biomass. Although depleted nitrate concentrations are generally expected at
622 coastal sites during the summer in density stratified water column due to phytoplankton assimilation, nitrate
623 concentrations at Friday Harbor in August of 2021 were upwards of 15 μM at the surface and 20 μM at 30 m
624 depth. Indeed, nitrate in the San Juan Channel is replete year-round, even at the surface, due to vigorous mixing
625 within the channel (Mackas and Harrison, 1997; Murray et al., 2015).

626 The region experiences tidal mixing, designating it as a well-mixed estuary with minimal density
627 stratification (Banas et al., 1999; Mackas and Harrison, 1997). The tidal influence is clearly identified from the
628 diurnal patterns of vertical hydrographic structure variability with the salinity/temperature gradients changing
629 with the tidal phase (Figure 6a and b). The tidal pumping drives vertical mixing between high nutrient deep water
630 from the Juan de Fuca Strait and fresher surface water from the Strait of Georgia (Banas et al., 1999; Lewis,
631 1978; Murray et al., 2015; Mackas and Harrison, 1997). Nutrient concentrations in the surface Georgia Strait vary
632 seasonally and are depleted during the summer at the stratified, fresher surface (Del Bel Belluz et al., 2021;
633 Mackas and Harrison, 1997). Our temperature-salinity plot in August 2021 reflects end-member mixing between
634 more saline/colder water from the Juan de Fuca Strait with fresher/warmer surface water from the Georgia Strait
635 (Figure S9; Banas et al., 1999). The influence of Georgia Strait surface water is recognized by the salinity
636 minima originating from the outflow of the Fraser River (Figures S10; Mackas and Harrison, 1997). The nitrate
637 profiles in August 2021, though collected with a lower vertical resolution, do show diurnal variability in vertical
638 gradients similar to salinity/temperature, consistent with the tidal mixing effect (Figure 6c).

639 The $\delta^{15}\text{N}$ of nitrate measured at stations near Friday Harbor also corroborate the mixing of nitrate-rich deeper
640 water with nitrate-deplete surface water from Georgia Strait. The apparent isotope effect for nitrate assimilation
641 in August 2021 was ~ 1.5 ‰, markedly lower than the canonical value of 5 ‰ associated with nitrate assimilation
642 by surface ocean phytoplankton communities (DiFiore et al., 2006; Sigman et al., 1999; Altabet and François,
643 1994). A low apparent isotope effect is consistent with two end-member mixing of lower $\delta^{15}\text{N}$, nitrate-rich water
644 with highly fractionated (high $\delta^{15}\text{N}$), low-nitrate water (Sigman et al., 1999). Highly fractionated nitrate, in turn,
645 likely originated from nutrient-depleted Georgia Strait surface waters entrained into the Channel Islands. The
646 linear relationship between salinity and nitrate concentration in August 2021 further substantiates physical
647 mixing as the dominant control on nitrate concentrations and isotope ratios in San Juan Channel (Figure S10;

648 Mackas and Harrison, 1997). Moreover, the $\delta^{15}\text{N}$ of nitrate was relatively uniform with depth, indicating effective
649 vertical mixing of the Georgia Strait and Juan de Fuca Strait water masses. The relatively slight decrease in
650 nitrate $\delta^{15}\text{N}$ with depth suggests a secondary influence of local nitrate assimilation on its concentration and
651 isotope ratios.

652 The corresponding $\delta^{15}\text{N}$ of SPOM at Friday Harbor covered a broad range, from 4.2 ‰ to 8.7 ‰ in August
653 2021. The depth distribution of SPOM did not mirror the corresponding nitrate $\delta^{15}\text{N}$ profile, as could otherwise
654 be expected. At the stratified near-surface (5 m) at station 1, the $\delta^{15}\text{N}$ of SPOM averaged 4.2 ‰ compared to 7.4
655 ‰ for nitrate. In the context of Rayleigh fractionation, this result suggests that particulate material at the surface
656 consisted primarily of the instantaneous product of nitrate assimilation (Mariotti et al., 1981). The lower $\delta^{15}\text{N}$
657 SPOM values could also reflect some degree of reliance on regenerated N species, which would result in $\delta^{15}\text{N}$ of
658 SPOM lower than that of incident nitrate (Fawcett et al., 2011; Lourey et al., 2003; Treibergs et al., 2014).
659 Deeper in the water column, the $\delta^{15}\text{N}$ of SPOM converged on the $\delta^{15}\text{N}$ of incident nitrate, between 6 and 7‰,
660 suggesting that SPOM derived from the complete consumption of an incident nitrate pool (even though nitrate
661 was present at these depths). Phytoplankton at these depths may thus have originated from surface water
662 entrained from the Strait of Georgia – where nitrate was completely utilized. The above dynamics complicate
663 validation of the offset between $\delta^{15}\text{N}$ of exported PON and coral-bound $\delta^{15}\text{N}$. Yet we find little evidence for
664 nitrate fractionation from partial assimilation on $\delta^{15}\text{N}$ of phytoplankton SPOM, which suggests that the $\delta^{15}\text{N}$
665 imparted on local *B. elegans* skeletons should reflect the $\delta^{15}\text{N}$ of nitrate entrained to the surface. The ~ 7‰
666 difference between coral skeleton $\delta^{15}\text{N}$ (~13.5‰) and the entrained nitrate (~6.5‰) is similar to the empirical
667 range of 7 - 9‰ reported for other CWC species, (e.g. *D. petusa*, Kiriakoulakis et al., 2005) and *D. dianthus*
668 (Wang et al. 2014) and suggests that *B. elegans* provides a record of the thermocline nitrate $\delta^{15}\text{N}$ and surface
669 nutrient dynamics at Friday Harbor.

670 **5. Conclusions and implications for paleo-reconstruction from coral $\delta^{15}\text{N}$**

671 We conclude that the solitary scleractinian cold water coral *B. elegans* in Friday Harbor, WA predominantly
672 derives nutrition from metazoan zooplankton prey. While our study was limited to a shallow field site, our
673 isotope feeding experiment, evaluated alongside previously published studies, points to the possibility that
674 deeper-dwelling CWCs could also rely on zooplankton prey as a fundamental component of their diet. SPOM
675 may contribute to these CWCs' diet, but it cannot be presumed to exclusively account for the large offset
676 between $\delta^{15}\text{N}$ of PON export and coral skeleton $\delta^{15}\text{N}$ documented by Wang et al. (2014). The $\delta^{15}\text{N}$ of skeletal

677 material recovered from coral archives is thus likely to be sensitive to local food web dynamics; for a given $\delta^{15}\text{N}$
678 of sinking PON exiting the surface ocean, the $\delta^{15}\text{N}$ recorded by CWC may differ among individuals of the same
679 species feeding on different zooplankton prey, depending on availability. In fact, Wang et al. (2014) did report a
680 “natural variability” of 1-1.5‰ within a single specimen that might have resulted from some variability of the
681 local food web on a short time scale of few years. Some studies have documented an increase in the degree of
682 carnivory of zooplankton with depth (Dodds et al., 2009; Vinogradov, 1962). For instance, Hannides et al. (2013)
683 recorded a 3.5 ‰ increase in zooplankton $\delta^{15}\text{N}$ from 150 m to 1000 m in the Subtropical North Pacific, with the
684 steepest rate of increase from 100 – 300 m. Koppelman et al. (2009) reported a similar pattern of
685 zooplankton $\delta^{15}\text{N}$ through the water column. These findings could explain previous reports of small but
686 resolvable (1-2 ‰) depth-dependencies of coral $\delta^{15}\text{N}$ (Wang et al. 2014) if corals feed predominantly on
687 zooplankton with depth-dependent degree of carnivory of zooplankton and increasing with depth $\delta^{15}\text{N}$. The $\delta^{15}\text{N}$
688 recorded in CWC skeletons also tends to differ among species by 1-2‰, as respective species occupy different
689 nutritional niches (Teece et al., 2011). The relationship between CWC species represented in fossil archives to
690 the depth structure of their zooplankton prey warrants further investigation.

691 Consideration of the possible dependence of coral-bound $\delta^{15}\text{N}$ on food web dynamics informs the questions
692 that can be competently addressed by this proxy. Although we do not have direct estimates of the $\delta^{15}\text{N}$ range that
693 can be expected from local food web variability, the scatter around the global compilation of Wang et al. (2014)
694 for coral-bound $\delta^{15}\text{N}$ of *D. dianthus* relative to the $\delta^{15}\text{N}$ of PON suggests that this range is modest, on the order of
695 ~1-2 ‰. Given this range, we suggest that the coral-bound $\delta^{15}\text{N}$ proxy will be most useful for reconstructing
696 larger environmental $\delta^{15}\text{N}$ signals and where chosen coral samples belong to the same species and are collected at
697 comparable depths as has already been successfully demonstrated by Wang et al. (2017), Studer et al. (2018) and
698 Chen et al. (2023). If used in this way, the broad geographic and temporal coverage afforded by CWCs, the
699 opportunity to measure multiple proxies from individual specimens and the imperviousness of coral-bound $\delta^{15}\text{N}$
700 to diagenetic alteration render it a valuable paleo-proxy for reconstructing marine N cycling.

701

702 **Data Availability** Data presented in this paper is available at: <https://www.bco-dmo.org/project/893811>

703

704 **Author Contribution** JG, AG, and MP conceptualized the research presented in this paper. JM and AG designed
705 and carried out culture experiments. MP and AC prepared coral samples for analysis. JM and VR analyzed
706 samples. JM, AG, JG and KD collected water samples, SPOM, and net tows. KD collected live corals for culture
707 experiments and field studies. JM and JG prepared the manuscript with contributions from all co-authors.

708

709 **Competing Interests:** The authors declare that they have no conflict of interest.

710

711 **Acknowledgements**

712 We are grateful to Friday Harbor Labs for their assistance with coral collections and field sampling, especially
713 Pema Kitaeff and Megan Dethier. We acknowledge the valued assistance of the Artemia Reference Center
714 (specifically Gilbert Van Stappen and Christ Mahieu). Coral culture experiments would not have been sustained
715 without the help of St. Olaf undergraduate students Rachel Raser, Joash Daniel, Qintiantian Nong, YiWynn
716 Chan, Mansha Haque, Natasia Preys and Miranda Lenz. We are also indebted to Dr. C. Tobias and P. Ruffino for
717 access to and assistance with the Elemental Analyzer Isotope Ratio Mass Spectrometer. This project was
718 funded by an NSF RUI award to A.G. (OCE-1949984), M.G.P (OCE-1949132) and J.G. (OCE-1949119).

719

720 **References**

- 721 Adams, T.S., Sterner, R.W. 2000. The effect of dietary nitrogen content on trophic level ¹⁵N enrichment. *Limnol.*
722 *Oceanogr.* 45, 601–607. <https://doi.org/10.4319/lo.2000.45.3.0601>
- 723 Adkins, J.F., Henderson, G.M., Wang, S.-L., O’Shea, S., Mokadem, F. 2004. Growth rates of the deep-sea
724 Scleractinia *Desmophyllum cristagalli* and *Enallopsammia rostrata*. *Earth and Planetary Science Letters*
725 227, 481-490. <https://doi.org/10.1016/j.epsl.2004.08.022>
- 726 Al-Moghrabi, S., Allemand, D. & Jaubert, J. 1993. Valine uptake by the scleractinian coral *Galaxea fascicularis*:
727 characterization and effect of light and nutritional status. *J Comp Physiol B* **163**, 355–362.
728 <https://doi.org/10.1007/BF00265638>
- 729 Altabet, M.A., 1988. Variations in nitrogen isotopic composition between sinking and suspended particles:
730 implications for nitrogen cycling and particle transformation in the open ocean. *Deep Sea Res. Part*
731 *Oceanogr. Res. Pap.* 35, 535–554. [https://doi.org/10.1016/0198-0149\(88\)90130-6](https://doi.org/10.1016/0198-0149(88)90130-6)
- 732 Altabet, M.A., Deuser, W.G., Honjo, S., Stienen, C., 1991. Seasonal and depth-related changes in the source of
733 sinking particles in the North Atlantic. *Nature* 354, 136–139. <https://doi.org/10.1038/354136a0>
- 734 Altabet, M.A., Francois, R., 1994. Sedimentary nitrogen isotopic ratio as a recorder for surface ocean nitrate
735 utilization. *Glob. Biogeochem. Cycles* 8, 103–116. <https://doi.org/10.1029/93GB03396>
- 736 Altabet, M., Higginson, M. & Murray, D. 2002. The effect of millennial-scale changes in Arabian Sea
737 denitrification on atmospheric CO₂. *Nature* **415**, 159–162. <https://doi.org/10.1038/415159a>
- 738 Ayliffe, L.K., Cerling, T.E., Robinson, T., West, A.G., Sponheimer, M., Passey, B.H., Hammer, J., Roeder, B.,
739 Dearing, M.D., Ehleringer, J.R., 2004. Turnover of carbon isotopes in tail hair and breath CO₂ of horses
740 fed an isotopically varied diet. *Oecologia* 139, 11–22. <https://doi.org/10.1007/s00442-003-1479-x>
- 741 Banas, N., Bricker, J., Carter, G., Gerdes, F., Martin, W., Nelson, E., Ross, T., Scansen, B., Simons, R., Wells,
742 M., 1999. Flow, Stratification, and mixing in San Juan Channel.
- 743 Beauchamp, K.A., 1989. Aspects of gametogenesis, development and planulation in laboratory populations of
744 solitary corals and corallimorpharian sea anemones (Ph.D.). University of California, Santa Cruz, United
745 States -- California.

- 746 Böhlke, J.K., Mroczkowski, S.J., Coplen, T.B., 2003. Oxygen isotopes in nitrate: new reference materials for
747 18O:17O:16O measurements and observations on nitrate-water equilibration. *Rapid Commun. Mass*
748 *Spectrom.* RCM 17, 1835–1846. <https://doi.org/10.1002/rem.1123>
- 749 Braman, R.S., Hendrix, S.A., 1989. Nanogram nitrite and nitrate determination in environmental and biological
750 materials by vanadium(III) reduction with chemiluminescence detection. *Anal. Chem.* 61, 2715–2718.
751 <https://doi.org/10.1021/ac00199a007>
- 752 Brandes, J.A., Devol, A.H., 2002. A global marine-fixed nitrogen isotopic budget: Implications for Holocene
753 nitrogen cycling. *Glob. Biogeochem. Cycles* 16, 67-1-67–14. <https://doi.org/10.1029/2001GB001856>
- 754 Bronk, D. A. 2002. Dynamics of DON. *Biogeochem. Mar. Dissolved Org. Matter* 153–249.
- 755 Brown, B. E., & Bythell, J. C. 2005. Perspectives on mucus secretion in reef corals. *Marine Ecology Progress*
756 *Series*, 296, 291–309. <http://www.jstor.org/stable/24868640>Cairns, S.D., 2007. Deep-water corals: an
757 overview with special reference to diversity and distribution of deep-water scleractinian corals. *Bull.*
758 *Mar. Sci.* 81, 311–322.
- 759 Carlier, A., Guilloux, E.L., Olu, K., Sarrazin, J., Mastrototaro, F., Taviani, M., Clavier, J., 2009. Trophic
760 relationships in a deep Mediterranean cold-water coral bank (Santa Maria di Leuca, Ionian Sea). *Mar.*
761 *Ecol. Prog. Ser.* 397, 125–137. <https://doi.org/10.3354/meps08361>
- 762 Carpenter, E. J., Harvey, H. R., Fry, B. & Capone, D. G. 1997. Biogeochemical tracers of the marine
763 cyanobacterium *Trichodesmium*. *Deep-Sea Res. I* 44, 27–38. [doi.org/10.1016/S0967-0637\(96\)00091-X](https://doi.org/10.1016/S0967-0637(96)00091-X)
- 764 Casciotti, K.L., Sigman, D.M., Hastings, M.G., Böhlke, J.K., Hilkert, A., 2002. Measurement of the oxygen
765 isotopic composition of nitrate in seawater and freshwater using the denitrifier method. *Anal. Chem.* 74,
766 4905–4912. <https://doi.org/10.1021/ac020113w>
- 767 Casciotti, K.L., Trull, T.W., Glover, D.M., Davies, D., 2008. Constraints on nitrogen cycling at the subtropical
768 North Pacific Station ALOHA from isotopic measurements of nitrate and particulate nitrogen. *Deep Sea*
769 *Res. Part II Top. Stud. Oceanogr.* 55, 1661–1672. <https://doi.org/10.1016/j.dsr2.2008.04.017>
- 770 Cathalot C, Van Oevelen D, Cox TJS, Kutti T, Lavaleye M., Duineveld G., Meysman F. J. R. 2015. Cold-water
771 coral reefs and adjacent sponge grounds: hotspots of benthic respiration and organic carbon cycling in the
772 deep sea. *Front Mar Sci* 2. <https://www.frontiersin.org/articles/10.3389/fmars.2015.00037>.
- 773 Cerling, T.E., Ayliffe, L.K., Dearing, M.D., Ehleringer, J.R., Passey, B.H., Podlesak, D.W., Torregrossa, A-M.,
774 West, A.G. 2007. Determining biological tissue turnover using stable isotopes: the reaction progress
775 variable. *Ecophysiology* 151, 175-189. <https://doi.org/10.1007/s00442-006-0571-4>
- 776 Chen, WH., Ren, H., Chiang, J.C.H. *et al.* Increased tropical South Pacific western boundary current transport
777 over the past century. *Nat. Geosci.* 16, 590–596 (2023). <https://doi.org/10.1038/s41561-023-01212-4>
- 778 Cheng, H., Adkins, J., Edwards, R.L., Boyle, E.A., 2000. U-Th dating of deep-sea corals. *Geochim. Cosmochim.*
779 *Acta* 64, 2401–2416. [https://doi.org/10.1016/S0016-7037\(99\)00422-6](https://doi.org/10.1016/S0016-7037(99)00422-6)
- 780 Crook, E.D., Cooper, H., Potts, D.C., Lambert, T., Paytan, A., 2013. Impacts of food availability and pCO₂ on
781 planulation, juvenile survival, and calcification of the azooxanthellate scleractinian coral *Balanophyllia*
782 *elegans*. *Biogeosciences* 10, 7599–7608. <https://doi.org/10.5194/bg-10-7599-2013>
- 783 Da Ros, Z., Dell’Anno, A., Fanelli, E., Angeletti, L., Taviani, M., Danovaro, R., 2022. Food preferences of
784 Mediterranean cold-water corals in captivity. *Front. Mar. Sci.* 9.

- 785 Del Bel Belluz, J., Peña, M.A., Jackson, J.M., Nemcek, N., 2021. Phytoplankton composition and environmental
786 drivers in the Northern Strait of Georgia (Salish Sea), British Columbia, Canada. *Estuaries Coasts* 44,
787 1419–1439. <https://doi.org/10.1007/s12237-020-00858-2>
- 788 De Pol-Holz R, Robinson RS, Hebbeln D, Sigman DM, Ulloa O. 2009. Controls on sedimentary nitrogen
789 isotopes along the Chile margin. *Deep Res Part II Top Stud Oceanogr* 56(16).
790 doi:10.1016/j.dsr2.2008.09.014
- 791 DiFiore, P.J., Sigman, D.M., Trull, T.W., Lourey, M.J., Karsh, K., Cane, G., Ho, R., 2006. Nitrogen isotope
792 constraints on subantarctic biogeochemistry. *J. Geophys. Res. Oceans* 111.
793 <https://doi.org/10.1029/2005JC003216>
- 794 Dodds, L.A., Black, K.D., Orr, H., Roberts, J.M., 2009. Lipid biomarkers reveal geographical differences in food
795 supply to the cold-water coral *Lophelia pertusa* (Scleractinia). *Mar. Ecol. Prog. Ser.* 397, 113–124.
796 <https://doi.org/10.3354/meps08143>
- 797 Doi, H., Akamatsu, F., González, A.L., 2017. Starvation effects on nitrogen and carbon stable isotopes of
798 animals: an insight from meta-analysis of fasting experiments. *R. Soc. Open Sci.* 4, 170633.
799 <https://doi.org/10.1098/rsos.170633>
- 800 Drake, J.L., Guillermic, M., Eagle, R.A., Jacobs, D.K., 2021. Fossil corals with various degrees of preservation
801 can retain information about biomineralization-related organic material. *Front. Earth Sci.* 9.
- 802 Druffel, E.R.M., 1997. Geochemistry of corals: Proxies of past ocean chemistry, ocean circulation, and climate.
803 *Proc. Natl. Acad. Sci.* 94, 8354–8361. <https://doi.org/10.1073/pnas.94.16.8354>
- 804 Duineveld, G.C.A., Lavaleye, M.S.S., Berghuis, E.M., 2004. Particle flux and food supply to a seamount cold-
805 water coral community (Galicia Bank, NW Spain). *Mar. Ecol. Prog. Ser.* 277, 13–23.
806 <https://doi.org/10.3354/meps277013>
- 807 Duineveld, G., Lavaleye, M., Bergman, M., Stigter, H., Mienis, F., 2007. Trophic structure of a cold-water coral
808 mound community (Rockall Bank, NE Atlantic) in relation to the near-bottom particle supply and current
809 regime. *Bull. Mar. Sci.* 81, 449–467.
- 810 Durham, J. W., and Barnard, J.L., 1952. Stony corals of the Eastern Pacific collected by the Velero III and Velero
811 IV. Allan Hancock Pacific Expeditions 16, 1-110.
- 812 Erler, D.V., Wang, X.T., Sigman, D.M., Scheffers, S.R., Shepherd, B.O., 2015. Controls on the nitrogen isotopic
813 composition of shallow water corals across a tropical reef flat transect. *Coral Reefs* 34, 329–338.
814 <https://doi.org/10.1007/s00338-014-1215-5>
- 815 Esri. "Ocean" [basemap]. Scale Not Given. " Ocean Basemap ". February 11, 2021.
816 [https://hub.arcgis.com/maps/CESPK::ocean-basemap/explore?location=35.956244%2C-](https://hub.arcgis.com/maps/CESPK::ocean-basemap/explore?location=35.956244%2C-111.078800%2C5.00)
817 [111.078800%2C5.00](https://hub.arcgis.com/maps/CESPK::ocean-basemap/explore?location=35.956244%2C-111.078800%2C5.00). (December, 2022).
- 818 Fadlallah, Y.H., 1983. Population Dynamics and Life History of a Solitary Coral, *Balanophyllia elegans*, from
819 Central California. *Oecologia* 58, 200–207.
- 820 Fautin, D.G., 2009. Structural diversity, systematics, and evolution of cnidae. *Toxicon, Cnidarian Toxins and*
821 *Venoms* 54, 1054–1064. <https://doi.org/10.1016/j.toxicon.2009.02.024>

- 822 Fawcett, S.E., Lomas, M.W., Casey, J.R., Ward, B.B., Sigman, D.M., 2011. Assimilation of upwelled nitrate by
823 small eukaryotes in the Sargasso Sea. *Nat. Geosci.* 4, 717–722. <https://doi.org/10.1038/ngeo1265>
- 824 Ferrier, M.D. 1991. Net uptake of dissolved free amino acids by four scleractinian corals. *Coral Reefs* 10, 183–
825 187. <https://doi.org/10.1007/BF00336772>
- 826 François, R., Altabet, M.A., Yu, E.-F., Sigman, D.M., Bacon, M.P., Frank, M., Bohrmann, G., Bareille, G.,
827 Labeyrie, L.D., 1997. Contribution of Southern Ocean surface-water stratification to low atmospheric
828 CO₂ concentrations during the last glacial period. *Nature* 389, 929–935. <https://doi.org/10.1038/40073>
- 829 Freiwald, A. 2002. Reef-Forming Cold-Water Corals. In: Wefer, G., Billett, D., Hebbeln, D., Jørgensen, B.B.,
830 Schlüter, M., van Weering, T.C.E. (eds) *Ocean Margin Systems*. Springer, Berlin, Heidelberg.
831 https://doi.org/10.1007/978-3-662-05127-6_23
- 832 Gagnon, A.C., Gothmann, A.M., Branson, O., Rae, J.W.B., Stewart, J.A., 2021. Controls on boron isotopes in a
833 cold-water coral and the cost of resilience to ocean acidification. *Earth and Planetary Science Letters*
834 554, 116662. <https://doi.org/10.1016/j.epsl.2020.116662>
- 835 Ganeshram, R. S., and Pedersen, T. F. 1998, Glacial-interglacial variability in upwelling and bioproductivity off
836 NW Mexico: Implications for Quaternary paleoclimate, *Paleoceanography*, 13(6), 634– 645,
837 doi:10.1029/98PA02508.
- 838 Garcia-Herrera, N., Cornils, A., Laudien, J., Niehoff, B., Höfer, J., Försterra, G., González, H.E., Richter, C.,
839 2022. Seasonal and diel variations in the vertical distribution, composition, abundance and biomass of
840 zooplankton in a deep Chilean Patagonian Fjord. *PeerJ* 10, e12823. <https://doi.org/10.7717/peerj.12823>
- 841 Genin, A., Dayton, P.K., Lonsdale, P.F., Spiess, F.N., 1986. Corals on seamount peaks provide evidence of
842 current acceleration over deep-sea topography. *Nature* 322, 59–61. <https://doi.org/10.1038/322059a0>
- 843 Gerrodette, T. 1981. Equatorial Submergence in a Solitary Coral, *Balanophyllia elegans*, and the Critical Life
844 Stage Excluding the Species from Shallow Water in the South. *Mar. Ecol. Prog. Series* 1, 227-235.
845 <http://www.jstor.org/stable/24812947>.
- 846 Gonfiantini, R., W. Stichler, and K. Rosanski 1995, Standards and Intercomparison. Materials Distributed by the
847 IAEA for Stable Isotope Measurements, Int. At. Energy Agency, Vienna.
- 848 Goodfriend, G.A., Hare, P.E., Druffel, E.R.M. 1992. Aspartic acid racemization and protein diagenesis in corals
849 over the last 350 years. *Geochim. Cosmochim. Acta* 56, 3847–3850. [https://doi.org/10.1016/0016-7037\(92\)90176-J](https://doi.org/10.1016/0016-7037(92)90176-J)
850
851
- 852 Gori, A., R. Grover, C. Orejas, S. Sikorski, and C. Ferrier-Pagès. 2014. Uptake of dissolved free amino acids by
853 four cold-water coral species from the Mediterranean Sea. *Deep Sea Res. Part II Top. Stud. Oceanogr.*
854 99: 42–50. doi:10.1016/j.dsr2.2013.06.007
- 855 Gothmann AM, Stolarski J, Adkins JF, et al. Fossil corals as an archive of secular variations in seawater
856 chemistry since the Mesozoic. *Geochim Cosmochim Acta*. 2015;160:188-208.
857 doi:<https://doi.org/10.1016/j.gca.2015.03.018>
- 858 Grover, R. Maguer, J-F, Allemand, D., Ferrier-Pagès, C. 2008. Uptake of dissolved free amino acids by the
859 scleractinian coral *Stylophora pistillata*. *J Exp Biol* 211 (6): 860–865. doi:
860 <https://doi.org/10.1242/jeb.012807>

- 861 Hannides, Cecelia C. S., Popp, Brian N., Choy, C. Anela, Drazen, Jeffrey C. 2013. Midwater zooplankton and
862 suspended particle dynamics in the North Pacific Subtropical Gyre: A stable isotope perspective,
863 *Limnology and Oceanography*, 58, doi: 10.4319/lo.2013.58.6.1931.
- 864 Hill, T.M., Myrvoid, C.R., Spero, H.J., Guilderson, T.P. 2014. Evidence for benthic and pelagic food web
865 coupling and carbon export from California margin bamboo coral archives. *Biogeosciences* 11, 3845–
866 3854. <https://doi.org/10.5194/bg-11-3845-2014>
- 867 Hines, S.K.V., Southon, J.R., Adkins, J.F. 2015. A high-resolution record of Southern Ocean intermediate water
868 radiocarbon over the past 30,000 years. *Earth and Planetary Science Letters* 432, 46-58.
869 <https://doi.org/10.1016/j.epsl.2015.09.038>
- 870 Hoegh-Guldberg, O., Williamson, J. Availability of two forms of dissolved nitrogen to the coral *Pocillopora*
871 *damicornis* and its symbiotic zooxanthellae. *Marine Biology* **133**, 561–570 (1999).
872 <https://doi.org/10.1007/s002270050496>
- 873 Höfer, J., González, H.E., Laudien, J., Schmidt, G.M., Häussermann, V., Richter, C., 2018. All you can eat: the
874 functional response of the cold-water coral *Desmophyllum dianthus* feeding on krill and copepods. *PeerJ*
875 6, e5872. <https://doi.org/10.7717/peerj.5872>
- 876 Horn, M.G., Robinson, R.S., Rynearson, T.A., Sigman, D.M., 2011. Nitrogen isotopic relationship between
877 diatom-bound and bulk organic matter of cultured polar diatoms. *Paleoceanography* 26.
878 <https://doi.org/10.1029/2010PA002080>
- 879 Kast, E.R., Stolper, D.A., Auderset, A., Higgins, J.A., Ren, H., Wang, X.T., Martínez-García, A., Haug, G.H.,
880 Sigman, D.M., 2019. Nitrogen isotope evidence for expanded ocean suboxia in the early Cenozoic.
881 *Science* 364, 386–389. <https://doi.org/10.1126/science.aau5784>
- 882 Kiriakoulakis, K., Fisher, E., Wolff, G.A., Freiwald, A., Grehan, A., Roberts, J.M., 2005. Lipids and nitrogen
883 isotopes of two deep-water corals from the North-East Atlantic: initial results and implications for their
884 nutrition, in: Freiwald, A., Roberts, J.M. (Eds.), *Cold-Water Corals and Ecosystems*, Erlangen Earth
885 Conference Series. Springer, Berlin, Heidelberg, pp. 715–729. https://doi.org/10.1007/3-540-27673-4_37
- 886 Knapp, A. N., K. L. Casciotti, and M. G. Prokopenko. 2018. Dissolved Organic Nitrogen Production and
887 Consumption in Eastern Tropical South Pacific Surface Waters. *Glob. Biogeochem. Cycles* **32**: 769–783.
888 doi:10.1029/2017GB005875
- 889 Knapp AN, DiFiore PJ, Deutsch C, Sigman DM, Lipschultz F. 2008. Nitrate isotopic composition between
890 Bermuda and Puerto Rico: Implications for N₂ fixation in the Atlantic Ocean. *Global Biogeochem Cycles*
891 22(3). doi:10.1029/2007GB003107
- 892 Koppelman, R., Böttger-Schnack, R., Möbius, J., Weikert, H., 2009. Trophic relationships of zooplankton in the
893 eastern Mediterranean based on stable isotope measurements. *Journal of Plankton Research* 31, 669-686.
- 894 Lasker, H.R., 1981. A comparison of the particulate feeding abilities of three species of Gorgonian soft coral.
895 *Mar. Ecol. Prog. Ser.* 5, 61–67.
- 896 Lewis, A.G., 1978. Concentrations of nutrients and chlorophyll on a cross-channel transect in Juan de Fuca Strait,
897 British Columbia. *J. Fish. Res. Board Can.* 35, 305–314. <https://doi.org/10.1139/f78-055>

- 898 Lewis, J.B., Price, W.S., 1975. Feeding mechanisms and feeding strategies of Atlantic reef corals. *J. Zool.* 176,
899 527–544. <https://doi.org/10.1111/j.1469-7998.1975.tb03219.x>
- 900 Li, T., Robinson, L.F., Chen, T., Wang, X.T., Burke, A., Rae, J.W.B., Pegrum-Haram, A., Knowles, T.D.J., Li,
901 G., Chen, J., Ng, H.C., Prokopenko, M., Rowland, G.H., Samperiz, A., Stewart, J.A., Southon, J.,
902 Spooner, P.T., 2020. Rapid shifts in circulation and biogeochemistry of the Southern Ocean during
903 deglacial carbon cycle events. *Science Advances* 6, eabb3807
904
- 905 Lourey, M.J., Trull, T.W., Sigman, D.M., 2003. Sensitivity of $\delta^{15}\text{N}$ of nitrate, surface suspended and deep
906 sinking particulate nitrogen to seasonal nitrate depletion in the Southern Ocean. *Glob. Biogeochem.*
907 *Cycles* 17. <https://doi.org/10.1029/2002GB001973>
- 908 Mackas, D.L., Harrison, P.J., 1997. Nitrogenous nutrient sources and sinks in the Juan de Fuca Strait/Strait of
909 Georgia/Puget Sound estuarine system: Assessing the potential for eutrophication. *Estuar. Coast. Shelf*
910 *Sci.* 44, 1–21. <https://doi.org/10.1006/ecss.1996.0110>
- 911 Maier, S.R., Bannister, R.J., van Oevelen, D., Kutti, T., 2020. Seasonal controls on the diet, metabolic activity,
912 tissue reserves and growth of the cold-water coral *Lophelia pertusa*. *Coral Reefs* 39, 173–187.
913 <https://doi.org/10.1007/s00338-019-01886-6>
- 914 Maier, S.R., Kutti, T., Bannister, R.J., van Breugel, P., van Rijswijk, P., van Oevelen, D., 2019. Survival under
915 conditions of variable food availability: Resource utilization and storage in the cold-water coral *Lophelia*
916 *pertusa*. *Limnol. Oceanogr.* 64, 1651–1671. <https://doi.org/10.1002/lno.11142>
- 917 Maier, S.R., Brooke, S., De Clippele, L.H., de Froe, E., van der Kaaden, A.-S., Kutti, T., Mienis, F., van Oevelen,
918 D., 2023. On the paradox of thriving cold-water coral reefs in the food-limited deep sea. *Biological*
919 *Reviews* 98, 1768–1795. <https://doi.org/10.1111/brv.12976>
- 920 Marconi D, Weigand AM, Rafter PA, Matthew R. McIlvin MR, Matthew Forbes, M Casciotti, KL Sigman, DM.
921 2015. Nitrate isotope distributions on the US GEOTRACES North Atlantic cross-basin section: Signals of
922 polar nitrate sources and low latitude nitrogen cycling. *Mar Chem.* 177:143-156.
923 doi:<https://doi.org/10.1016/j.marchem.2015.06.007>
- 924 Margolin, A. R., L. F. Robinson, A. Burke, R. G. Waller, K. M. Scanlon, M. L. Roberts, M. E. Auro, and T. van
925 de Flieddt. 2014. Temporal and spatial distributions of cold-water corals in the Drake Passage: Insights
926 from the last 35,000 years. *Deep Sea Res. Part II Top. Stud. Oceanogr.* 99: 237–248.
927 doi:10.1016/j.dsr2.2013.06.008
- 928 Mariotti, A., Germon, J.C., Hubert, P., Kaiser, P., Letolle, R., Tardieux, A., Tardieux, P., 1981. Experimental
929 determination of nitrogen kinetic isotope fractionation: Some principles; illustration for the
930 denitrification and nitrification processes. *Plant Soil* 62, 413–430. <https://doi.org/10.1007/BF02374138>
- 931 Martínez del Rio, C., Carleton, S.A., 2012. How fast and how faithful: the dynamics of isotopic incorporation
932 into animal tissues. *J. Mammal.* 93, 353–359. <https://doi.org/10.1644/11-MAMM-S-165.1>
- 933 McCutchan Jr, J.H., Lewis Jr, W.M., Kendall, C., McGrath, C.C., 2003. Variation in trophic shift for stable
934 isotope ratios of carbon, nitrogen, and sulfur. *Oikos* 102, 378–390. <https://doi.org/10.1034/j.1600-0706.2003.12098.x>
935

- 936 McIlvin, M.R., Casciotti, K.L., 2011. Technical Updates to the Bacterial Method for Nitrate Isotopic Analyses.
937 Anal. Chem. 83, 1850–1856. <https://doi.org/10.1021/ac1028984>
- 938 McMahon, K.W., Williams, B., Guilderson, T.P., Glynn, D.S., McCarthy, M.D., 2018. Calibrating amino acid
939 $\delta^{13}\text{C}$ and $\delta^{15}\text{N}$ offsets between polyp and protein skeleton to develop proteinaceous deep-sea corals as
940 paleoceanographic archives. *Geochim. Cosmochim. Acta* 220, 261–275.
941 <https://doi.org/10.1016/j.gca.2017.09.048>
- 942 Middelburg, J., Mueller, C., Veuger, B. Larsson, A. I., Form, A., van Oevelen, D 2016.. Discovery of symbiotic
943 nitrogen fixation and chemoautotrophy in cold-water corals. *Sci Rep* 5, 17962 (2016).
944 <https://doi.org/10.1038/srep17962>
- 945 Miller, M., 1995. Growth of a temperate coral: effects of temperature, light, depth, and heterotrophy. *Mar. Ecol.*
946 *Prog. Ser.* 122, 217–225. <https://doi.org/10.3354/meps122217>
- 947 Minagawa, M., Wada, E., 1984. Stepwise enrichment of ^{15}N along food chains: Further evidence and the relation
948 between $\delta^{15}\text{N}$ and animal age. *Geochim. Cosmochim. Acta* 48, 1135–1140.
949 [https://doi.org/10.1016/0016-7037\(84\)90204-7](https://doi.org/10.1016/0016-7037(84)90204-7)
- 950 Mortensen P.B., (2001) Aquarium observations on the deep-water coral *Lophelia pertusa* (L., 1758) (scleractinia)
951 and selected associated invertebrates, *Ophelia*, 54:2, 83-104, DOI: 10.1080/00785236.2001.10409457
- 952 Muhs, D.R., Kennedy, G.L., Rockwell, T.K., 1994. Uranium-Series Ages of Marine Terrace Corals from the
953 Pacific Coast of North America and Implications for Last-Interglacial Sea Level History. *Quaternary*
954 *Research* 42, 72–87. <https://doi.org/10.1006/qres.1994.1055>
- 955 Mueller, C.E., Larsson, A.I., Veuger, B., Middelburg, J.J., van Oevelen, D., 2014. Opportunistic feeding on
956 various organic food sources by the cold-water coral *Lophelia pertusa*. *Biogeosciences* 11, 123–133.
957 <https://doi.org/10.5194/bg-11-123-2014>
- 958 Murray, J.W., Roberts, E., Howard, E., O'Donnell, M., Bantam, C., Carrington, E., Foy, M., Paul, B., Fay, A.,
959 2015. An inland sea high nitrate-low chlorophyll (HNLC) region with naturally high pCO_2 . *Limnol.*
960 *Oceanogr.* 60, 957–966. <https://doi.org/10.1002/lno.10062>
- 961 Muscatine, L., Goiran, C., Land, L., Jaubert, J., Cuif, J.-P., Allemand, D., 2005. Stable isotopes ($\delta^{13}\text{C}$ and $\delta^{15}\text{N}$)
962 of organic matrix from coral skeleton. *Proc. Natl. Acad. Sci.* 102, 1525–1530.
963 <https://doi.org/10.1073/pnas.0408921102>
- 964 Naumann, M.S., Orejas, C., Wild, C., Ferrier-Pagès, C., 2011. First evidence for zooplankton feeding sustaining
965 key physiological processes in a scleractinian cold-water coral. *J. Exp. Biol.* 214, 3570–3576.
966 <https://doi.org/10.1242/jeb.061390>
- 967 Naumann, M.S., Tolosa, I., Taviani, M., Grover, R., Ferrier-Pagès, C., 2015. Trophic ecology of two cold-water
968 coral species from the Mediterranean Sea revealed by lipid biomarkers and compound-specific isotope
969 analyses. *Coral Reefs* 34, 1165–1175. <https://doi.org/10.1007/s00338-015-1325-8>
- 970 Pride C, Thunell R, Sigman D, Keigwin L, Altabet M, Tappa E. 1999. Nitrogen isotopic variations in the Gulf of
971 California since the Last Deglaciation: Response to global climate change. *Paleoceanography* 14(3).
972 doi:10.1029/1999PA900004

- 973 Purser A, Larsson AI, Thomsen L, van Oevelen D. 2010. The influence of flow velocity and food concentration
 974 on *Lophelia pertusa* (Scleractinia) zooplankton capture rates. *J Exp Mar Bio Ecol.* 395(1):55-62.
 975 doi:<https://doi.org/10.1016/j.jembe.2010.08.013>
- 976 Rae, J.W.B. 2018. Boron Isotopes in Foraminifera: Systematics, Biomineralisation, and CO₂ Reconstruction. In:
 977 Marschall, H., Foster, G. (eds) Boron Isotopes. Advances in Isotope Geochemistry. Springer, Cham.
 978 https://doi.org/10.1007/978-3-319-64666-4_5
- 979 Rangel, M.S., Erler, D., Tagliafico, A., Cowden, K., Scheffers, S., Christidis, L., 2019. Quantifying the transfer
 980 of prey $\delta^{15}\text{N}$ signatures into coral holobiont nitrogen pools. *Mar. Ecol. Prog. Ser.* 610, 33–49.
 981 <https://doi.org/10.3354/meps12847>
- 982 Ren, H., Sigman, D.M., Meckler, A.N., Plessen, B., Robinson, R.S., Rosenthal, Y., Haug, G.H., 2009.
 983 Foraminiferal Isotope Evidence of Reduced Nitrogen Fixation in the Ice Age Atlantic Ocean. *Science*
 984 323, 244–248. <https://doi.org/10.1126/science.1165787>
- 985 Reynaud, S., Martinez, P., Houlbrèque, F., Billy, I., Allemand, D., Ferrier-Pagès, C., 2009. Effect of light and
 986 feeding on the nitrogen isotopic composition of a zooxanthellate coral: role of nitrogen recycling. *Mar.*
 987 *Ecol. Prog. Ser.* 392, 103–110. <https://doi.org/10.3354/meps08195>
- 988 Roberts, J.M., Wheeler, A.J., Freiwald, A., 2006. Reefs of the deep: The biology and geology of cold-water coral
 989 ecosystems. *Science* 312, 543–547. <https://doi.org/10.1126/science.1119861>
- 990 Robinson, R.S., Kienast, M., Albuquerque, A.L., Altabet, M., Contreras, S., Holz, R.D.P., Dubois, N., Francois,
 991 R., Galbraith, E., Hsu, T.-C., Ivanochko, T., Jaccard, S., Kao, S.-J., Kiefer, T., Kienast, S., Lehmann, M.,
 992 Martinez, P., McCarthy, M., Möbius, J., Pedersen, T., Quan, T.M., Ryabenko, E., Schmittner, A.,
 993 Schneider, R., Schneider-Mor, A., Shigemitsu, M., Sinclair, D., Somes, C., Studer, A., Thunell, R., Yang,
 994 J.-Y., 2012. A review of nitrogen isotopic alteration in marine sediments. *Paleoceanography* 27.
 995 <https://doi.org/10.1029/2012PA002321>
- 996 Robinson LF, Adkins JF, Frank N, Gagnon, A.C., Prouty, N.G., Roark, B. van de Flierdt, T. 2014. The
 997 geochemistry of deep-sea coral skeletons: A review of vital effects and applications for
 998 palaeoceanography. *Deep Sea Res Part II Top Stud Oceanogr.* 99:184-198.
 999 doi:<https://doi.org/10.1016/j.dsr2.2013.06.005>
- 1000 Robinson RS, Sigman DM. 2008. Nitrogen isotopic evidence for a poleward decrease in surface nitrate within the
 1001 ice age Antarctic. *Quat Sci Rev.* 27(9-10). doi:10.1016/j.quascirev.2008.02.005
- 1002 Robinson, R.S., Smart, S.M., Cybulski, J.D., McMahon, K.W., Marcks, B., Nowakowski, C., 2023. Insights from
 1003 fossil-bound nitrogen isotopes in diatoms, foraminifera, and corals. *Annu. Rev. Mar. Sci.* 15, null.
 1004 <https://doi.org/10.1146/annurev-marine-032122-104001>
- 1005 Ryan, W. B. F., S.M. Carbotte, J. Coplan, S. O'Hara, A. Melkonian, R. Arko, R.A. Weissel, V. Ferrini, A.
 1006 Goodwillie, F. Nitsche, J. Bonczkowski, R. Zemsky, 2009. Global Multi-Resolution Topography
 1007 (GMRT) synthesis data set, *Geochem. Geophys. Geosyst.*, 10, Q03014, doi:10.1029/2008GC002332.
- 1008 Saino, T., Hattori, A., 1987. Geographical variation of the water column distribution of suspended particulate
 1009 organic nitrogen and its ^{15}N natural abundance in the Pacific and its marginal seas. *Deep Sea Res. A* 34,
 1010 807–827. [https://doi.org/10.1016/0198-0149\(87\)90038-0](https://doi.org/10.1016/0198-0149(87)90038-0)

- 1011 Scrimgeour, C.M., Gordon, S.C., Handley, L.L., Woodford, J.A.T., 1995. Trophic levels and anomalous $\delta^{15}\text{N}$ of
1012 insects on raspberry (*Rubus Idaeus* L.). *Isotopes Environ. Health Stud.* 31, 107–115.
1013 <https://doi.org/10.1080/10256019508036256>
- 1014 Sebens, K.P., Vandersall, K.S., Savina, L.A., Graham, K.R., 1996. Zooplankton capture by two scleractinian
1015 corals, *Madracis mirabilis* and *Montastrea cavernosa*, in a field enclosure. *Mar. Biol.* 127, 303–317.
1016 <https://doi.org/10.1007/BF00942116>
- 1017 Sherwood, O.A., Heikoop, J.M., Scott, D.B., Risk, M.J., Guilderson, T.P., McKinney, R.A., 2005. Stable isotopic
1018 composition of deep-sea gorgonian corals *Primnoa* spp.: a new archive of surface processes. *Mar. Ecol.*
1019 *Prog. Ser.* 301, 135–148. <https://doi.org/10.3354/meps301135>
- 1020 Sherwood, O.A., Jamieson, R.E., Edinger, E.N., Wareham, V.E., 2008. Stable C and N isotopic composition of
1021 cold-water corals from the Newfoundland and Labrador continental slope: Examination of trophic, depth
1022 and spatial effects. *Deep Sea Res. Part Oceanogr. Res. Pap.* 55, 1392–1402.
1023 <https://doi.org/10.1016/j.dsr.2008.05.013>
- 1024 Sherwood, O.A., Thresher, R.E., Fallon, S.J., Davies, D.M., Trull, T.W., 2009. Multi-century time-series of ^{15}N
1025 and ^{14}C in bamboo corals from deep Tasmanian seamounts: evidence for stable oceanographic
1026 conditions. *Mar. Ecol. Prog. Ser.* 397, 209–218. <https://doi.org/10.3354/meps08166>
- 1027 Sigman, D.M., Altabet, M.A., McCorkle, D.C., Francois, R., Fischer, G., 1999. The $\delta^{15}\text{N}$ of nitrate in the
1028 Southern Ocean: Consumption of nitrate in surface waters. *Glob. Biogeochem. Cycles* 13, 1149–1166.
1029 <https://doi.org/10.1029/1999GB900038>
- 1030 Sigman, D., Boyle, E. Glacial/interglacial variations in atmospheric carbon dioxide. 2000. *Nature* 407, 859–869
1031 (2000). <https://doi.org/10.1038/35038000>
- 1032 Sigman, D.M., Casciotti, K.L., Andreani, M., Barford, C., Galanter, M., Böhlke, J.K., 2001. A Bacterial method
1033 for the nitrogen isotopic analysis of nitrate in seawater and freshwater. *Anal. Chem.* 73, 4145–4153.
1034 <https://doi.org/10.1021/ac010088e>
- 1035 Sigman, D.M., Fripiat, F., 2019. *Nitrogen Isotopes in the Ocean*, in: Cochran, J.K., Bokuniewicz, H.J., Yager,
1036 P.L. (Eds.), *Encyclopedia of Ocean Sciences (Third Edition)*. Academic Press, Oxford, pp. 263–278.
1037 <https://doi.org/10.1016/B978-0-12-409548-9.11605-7>
- 1038 Soetaert, K., Mohn, C., Rengstorf, A., Grehan, A., van Oevelen, D., 2016. Ecosystem engineering creates a direct
1039 nutritional link between 600-m deep cold-water coral mounds and surface productivity. *Sci. Rep.* 6,
1040 35057. <https://doi.org/10.1038/srep35057>
- 1041 Spero, H.J., Andreasen, D.J., Sorgeloos, P., 1993. Carbon and nitrogen isotopic composition of different strains
1042 of *Artemia* sp. *Int. J. Salt Lake Res.* 2, 133. <https://doi.org/10.1007/BF02905905>
- 1043 Studer, A.S., Sigman, D.M., Martinez-Garcia, A., Thole, L.M., Michel, E., Jaccard, S.L., Lippolds, J.A., Mazaud,
1044 A., Wang, X.C.T., Robinson, L.F., Adkins, J.F., Haug, G.H., 2018. Increased nutrient supply to the
1045 Southern Ocean during the Holocene and its implications for the pre-industrial atmospheric CO_2 rise.
1046 *Nat Geosci* 11, 756–761
- 1047 Tanaka, Y., Miyajima, T., Koike, I., Hayashibara, T., Ogawa, H., 2006. Translocation and conservation of
1048 organic nitrogen within the coral-zooxanthella symbiotic system of *Acropora pulchra*, as demonstrated

- 1049 by dual isotope-labeling techniques. *J. Exp. Mar. Biol. Ecol.* 336, 110–119.
1050 <https://doi.org/10.1016/j.jembe.2006.04.011>
- 1051 Tanaka, Y., Suzuki, A., Sakai, K., 2018. The stoichiometry of coral-dinoflagellate symbiosis: carbon and nitrogen
1052 cycles are balanced in the recycling and double translocation system. *ISME J.* 12, 860–868.
1053 <https://doi.org/10.1038/s41396-017-0019-3>
- 1054 Teece, M.A., Estes, B., Gelsleichter, E., Lirman, D., 2011. Heterotrophic and autotrophic assimilation of fatty
1055 acids by two scleractinian corals, *Montastraea faveolata* and *Porites astreoides*. *Limnol. Oceanogr.* 56,
1056 1285–1296. <https://doi.org/10.4319/lo.2011.56.4.1285>
- 1057 Thiagarajan N., Subhas A. V., Southon J. R., Eiler J. M. and Adkins J. F. 2014. Abrupt pre-Bolling-Allerod
1058 warming and circulation changes in the deep ocean. *Nature* 511, 75–78.
1059 <https://doi.org/10.1038/nature13472>
- 1060 Thiem, Ø., Ravagnan, E., Fosså, J.H., Berntsen, J., 2006. Food supply mechanisms for cold-water corals along a
1061 continental shelf edge. *J. Mar. Syst.* 60, 207–219. <https://doi.org/10.1016/j.jmarsys.2005.12.004>
- 1062 Thomas, S.M., Crowther, T.W., 2015. Predicting rates of isotopic turnover across the animal kingdom: a
1063 synthesis of existing data. *J. Anim. Ecol.* 84, 861–870. <https://doi.org/10.1111/1365-2656.12326>
- 1064 Treibergs, L.A., Fawcett, S.E., Lomas, M.W., Sigman, D.M., 2014. Nitrogen isotopic response of prokaryotic and
1065 eukaryotic phytoplankton to nitrate availability in Sargasso Sea surface waters. *Limnol. Oceanogr.* 59,
1066 972–985. <https://doi.org/10.4319/lo.2014.59.3.0972>
- 1067 Tsounis G, Orejas C, Reynaud S, JM G, Allemand D, Ferrier-Pagès C. 2010. Prey-capture rates in four
1068 Mediterranean cold water corals . *Mar Ecol Prog Ser.* 398:149-155. <https://doi.org/10.3354/meps08312>
- 1069 van Oevelen, P., Duineveld, G., Lavaleye, M., Mienis, Furu, Soetaert, Karline, H., Carlo H. R., 2009. The cold-
1070 water coral community as hotspot of carbon cycling on continental margins: A food-web analysis from
1071 Rockall Bank (northeast Atlantic), *Limnology and Oceanography*, 54, doi: 10.4319/lo.2009.54.6.1829.
- 1072 Vinogradov, M. E. Feeding of the deep-sea zooplankton. 1962. *Rapp. Pv. Reun. Cons. Perm. Int. Exp. Mer.* 153,
1073 114–120.
- 1074 Wang, X.T., Prokopenko, M.G., Sigman, D.M., Adkins, J.F., Robinson, L.F., Ren, H., Oleynik, S., Williams, B.,
1075 Haug, G.H., 2014. Isotopic composition of carbonate-bound organic nitrogen in deep-sea scleractinian
1076 corals: A new window into past biogeochemical change. *Earth Planet. Sci. Lett.* 400, 243–250.
1077 <https://doi.org/10.1016/j.epsl.2014.05.048>
- 1078 Wang, X.T., Sigman, D.M., Prokopenko, M.G., Adkins, J.F., Robinson, L.F., Hines, S.K., Chai, J., Studer, A.S.,
1079 Martínez-García, A., Chen, T., Haug, G.H., 2017. Deep-sea coral evidence for lower Southern Ocean
1080 surface nitrate concentrations during the last ice age. *Proc. Natl. Acad. Sci.* 114, 3352–3357.
1081 <https://doi.org/10.1073/pnas.1615718114>
- 1082 Webb, S., Hedges, R., Simpson, S., 1998. Diet quality influences the $\delta^{13}\text{C}$ and $\delta^{15}\text{N}$ of locusts and their
1083 biochemical components. *J. Exp. Biol.* 201, 2903–2911. <https://doi.org/10.1242/jeb.201.20.2903>
- 1084 Weigand, M.A., Foriel, J., Barnett, B., Oleynik, S., Sigman, D.M., 2016. Updates to instrumentation and
1085 protocols for isotopic analysis of nitrate by the denitrifier method. *Rapid Commun. Mass Spectrom.* 30,
1086 1365–1383. <https://doi.org/10.1002/rcm.7570>

- 1087 Williams, B., and Grottoli, A. G. 2010. Recent shoaling of the nutricline and thermocline in the western tropical
1088 Pacific, *Geophys. Res. Lett.*, 37, L22601, doi:10.1029/2010GL044867.
- 1089 Zhang, R., X. T. Wang, H. Ren, J. Huang, M. Chen, and D. M. Sigman. 2020. Dissolved Organic Nitrogen
1090 Cycling in the South China Sea From an Isotopic Perspective. *Glob. Biogeochem. Cycles* 34:
1091 e2020GB006551. doi:10.1029/2020GB006551
- 1092 Zhou, M., Granger, J., Chang, B.X., 2022. Influence of sample volume on nitrate N and O isotope ratio analyses
1093 with the denitrifier method. *Rapid Commun. Mass Spectrom.* 36, e9224.
1094 <https://doi.org/10.1002/rcm.9224>